

Visualization-aided Multi-Criteria Decision-Making using Interpretable Self-Organizing Maps

Deepanshu Yadav^{a,*}, Deepak Nagar^a, Palaniappan Ramu^a and Kalyanmoy Deb^b

^aDepartment of Engineering Design, Indian Institute of Technology Madras, Chennai, India

^bDepartment of Electrical and Computer Engineering, Michigan State University, East Lansing, USA

COIN Report Number 2023011

ARTICLE INFO

Keywords:

Multiple criteria analysis
Evolutionary multi-criterion optimization
Multi-criteria decision making
NIMBUS
Self-Organizing Maps

ABSTRACT

In multi-criterion optimization, decision-makers (DMs) are not often interested in the complete Pareto-optimal front. Instead, they have preferences favoring specific parts of the front. Multi-criterion decision-making (MCDM) literature provides a plethora of approaches for introducing DM's preference information in an interactive manner to solve multi-criterion optimization problems. Interactions with DMs can be aided with a user-friendly visualization method or by using special data analysis procedures. An earlier study has indicated the use of self-organizing maps (SOM) as a tool for analyzing Pareto-optimal solutions. In this paper, we demonstrate how a specific MCDM method – NIMBUS – can be executed with the interpretable SOM (iSOM) approach iteratively to arrive at one or more preferred solutions. A visual illustration of the entire high-dimensional search space into multiple reduced two-dimensional spaces allows DMs to have a better understanding of the interactions of the objectives and constraints independently, and execute the NIMBUS decision-making procedure with a more wholistic approach. The paper demonstrates the proposed method on a number of multi- and many-objective numerical and engineering problems. The approach is now ready to be integrated with other popular MCDM methods.

1. Introduction

OPTIMIZATION problems are now increasingly being solved for more than one criterion for several reasons. First, most practical problems are better posed as a multi-criterion optimization problem, as often the resulting optimal solution(s) must conform to several conflicting functional goals (such as cost, quality, emission, waste, etc.). Second, despite the ultimate choice of a single preferred optimal solution, multiple trade-off optimal solutions, which become the outcome of a multi-criterion optimization problem, provide relevant knowledge of possible alternate solutions to the decision-makers (DMs) for them to be on top of guesses and prejudices. Finding a set of trade-off optimal solutions (known as Pareto-optimal solutions in the parlance of multi-criterion optimization) has mostly been followed using two broad philosophies of optimization: (i) generative approach (Miettinen, 2012; Steuer, 1986; Chankong and Haimes, 2008) in which a single Pareto-optimal solution is found one at a time by solving a parameterized scalarization of multiple criteria and (ii) simultaneous approach (Deb, 2011; Coello et al., 2007) in which multiple Pareto-optimal solutions are found in a single run of the algorithm. Evolutionary Multi-objective Optimization (EMO) methodologies, proposed in the early nineties fall in the second category of algorithms, which are used to solve more than three-objective problems (Deb and Jain, 2014; Li et al., 2014; Yuan et al., 2015).

In addition to optimization algorithms to find multiple Pareto optimal solutions, there is a need for multi-criterion decision-making (MCDM) task which can follow the optimization task or be applied interactively with the optimization task (Ma et al., 1999). Starting in the early seventies, various MCDM approaches were proposed to systematically involve one or more DMs in providing preference information, either in terms of objective preferences irrespective of solutions, preference of one solution over another in a pairwise comparison based on their objective and constraint

*Corresponding author

✉ deepanshu.yadav380@gmail.com (D. Yadav); deepakn297@gmail.com (D. Nagar); palramu@iitm.ac.in (P. Ramu); kdeb@egr.msu.edu (K. Deb)

🌐 <https://ed.iitm.ac.in/~palramu/> (P. Ramu); <https://www.egr.msu.edu/~kdeb/> (K. Deb)

ORCID(s): 0000-0003-1841-8942 (D. Yadav); 0000-0002-5268-0226 (D. Nagar); 0000-0001-9704-2087 (P. Ramu); 0000-0001-7402-9939 (K. Deb)

¹Postal address: Department of Engineering Design, Indian Institute of Technology Madras, Chennai, India, 600 036

values, or by other means. These interactive MCDM approaches usually formulate a scalarized version of the multi-criterion optimization problems in an interactive manner. The scalarization process requires DM's preference information and thereby largely depends on the solutions being compared and their properties. To properly formulate a scalarized problem, it is extremely helpful to the DMs to visualize the solutions well in a low-dimensional mapped search space along with trade-off information of objectives, their nearness to constraint boundaries, and other relevant information assisting in the decision-making process. It is needless to say that an efficient decision-making process is less likely to be completely algorithmic; rather, it should be as procedural as possible but must accompany different analysis tools providing relevant trade-off information, but importantly it must be guided by human decision-makers having a direct stake in the problem (Branke et al., 2009).

Thus, it is clear from the above discussion that a multi-criterion problem-solving task cannot be a pure algorithmic exercise of finding just any optimal solution in the search space, but must involve human decision-makers, their perception of solutions through preferences of objectives and constraints involved in the problem (Ho et al., 2010; Sinha et al., 2014). The latter task can be aided by a proper understanding of the location of key solutions in the search space, the trade-off they produce among objectives and their closeness to constraint boundaries. This decision-making task can be better achieved through the use of modern data analysis and visualization methods that are easily understandable to human decision-makers. This paper demonstrates such an aspect of decision-making on a popularly used MCDM approach using a recent data analysis and visualization tool on several three to ten-objective problems.

There exist many systematic MCDM methods for achieving the optimization and decision-making tasks together. The use of an aspiration objective point and a preference direction vector in the Achievement Scalarization Function (ASF) approach (Wierzbicki, 1980, 1999) is used to scalarize multiple objectives into a single objective, thereby producing a single optimal solution in the end. ASF and its augmented version (AASF) (Miettinen, 2012) are extensively used to develop a number of MCDM methods, such as surrogate worth trade-off (SWT) method (Hall and Haimes, 1976), GUESS method (Buchanan, 1997), satisficing trade-off method (STOM) (Nakayama and Sawaragi, 1984), Pareto-race method (Korhonen and Wallenius, 1988; Korhonen and Yu, 2000), among others. These methods systematically change either the aspiration point or the preference direction vector in an iteration depending on the solution obtained at the previous iteration. Upon solving the AASF formulation, for example, only one solution (\mathbf{x}_{ASF}) is obtained. However, EMO methods (such as reference point-based methods) can be used to generate K additional solutions ($\mathbf{X}_{EMO} = \{\mathbf{x}^{(1)}, \mathbf{x}^{(2)}, \dots, \mathbf{x}^{(K)}\}$) in the vicinity of the single solution (\mathbf{x}_{ASF}). Availability of such a multiple solution set (\mathbf{X}_{EMO}) permits the DM to compare these solutions and select the most preferred one amongst them as an alternative solution instead of selecting just one (\mathbf{x}_{ASF}). This provides flexibility to the DM in selecting his/her preferred solution(s). On some occasions, EMO methods were shown to follow a specific MCDM approach to find multiple preferred solutions as a further process of providing flexibility in the scalarization process. Reference point-based NSGA-II (R-NSGA-II) (Deb and Jain, 2014), reference direction-based NSGA-II (Deb and Kumar, 2007a), light beam approach (Deb and Kumar, 2007b; Jaszkiewicz and Słowiński, 1999) are some such hybrid EMO-MCDM methods. Branke et al. (2015) allows the DMs to rank a single pair of solutions at regular intervals by learning a value function based on DMs' preferences. This preference information updates the algorithms' internal value function models and speeds up the evolution to arrive at the aspiration level. Branke et al. (2016) used the Choquet integral and proposed an interactive procedure that involves preference information in terms of pairwise comparisons.

Wang et al. (2015a) extensively discussed the decomposition-based methods and highlighted that the decomposition-based algorithms using pre-defined weights suffer from the issue of problem geometry. Although this issue can be handled by employing adaptive weights (Siwei et al., 2011; Gu et al., 2012; Qi et al., 2014), there is the possibility that the adaptive weights degrade the algorithm's convergence speed often on many-objective optimization problems. Highlighting the limitations of the decomposition-based methods, Wang et al. (2015a) proposed a preference-inspired co-evolutionary algorithm using weights (PICEA-w) that is less sensitive to the problem geometry. In this method, the weights are co-evolved with candidate solutions during the search process. Köksalan and Karahan (2010) proposed an interactive MCDM technique named iTDEA. This interactive MCDM technique utilizes the concept of a territory-defining evolutionary algorithm (TDEA) proposed by Karahan and Köksalan (2010). iTDEA technique allows DMs to apply their preferences on a set of representative Pareto optimal solutions interactively. In each iteration, a territory is defined around the preferred solution and a dense set of solutions is computed around it. The algorithm stops once the aspiration level of DM is obtained. Kaliszewski et al. (2012) proposed and formulated the expression for the lower and upper bounds on objectives or goals corresponding to the DM's preference. The accuracy of the lower and upper bounds is updated and controlled within the evolutionary computation framework. Wang et al. (2015b) proposed an interactive MCDM technique termed as brushing technique utilizing the concept of a preference-inspired

co-evolutionary algorithm using goals called PICEA-g (Wang et al., 2013). The brushing technique allows the DMs to provide their preferences by drawing in the objective function space unlike providing the numbers in the case of utility functions such as ASF and AASF. The implementation of interactive approaches using other MCDM techniques is recently studied in Kadziński et al. (2020); Tomczyk and Kadziński (2019).

The Non-differentiable Interactive Multiobjective BUNDLE-based optimization System (NIMBUS) is another interactive multi-criterion optimization and decision-making approach proposed in Miettinen and Mäkelä (1995) and is the focus of this paper. It starts with a single Pareto-optimal solution and works iteratively to arrive at another preferred Pareto-optimal solution satisfying DM's satisfaction level on different objectives and constraints. At each iteration, the DM can classify all conflicting objectives into five classes, each indicating different levels of satisfaction. For example, certain objectives may require to be improved further from their values at the current solution, or certain objectives may be allowed to deteriorate within specific limits for the improvement of some other objectives to take place, or certain objectives can be changed to any extent possible, as in the present context, they are not as important as the former two classes, and so on. Once such preference information is provided by the human DMs based on their desire and perception of an acceptable solution, scalarized single-objective formulation/s of the problem are formulated and solved to find an alternative solution. A feasibility check is always enforced to produce feasible solutions. The new solutions are compared with the previous solution(s), and a single solution is chosen to advance to the next iteration. The process is terminated when the DMs have found a satisfactory solution or a predefined number of iterations are elapsed.

It is clear from the above discussion that the progress of the entire process depends on DM's classification of objectives into different classes and the choice of a solution among a few at the end of each iteration. While there is no absolute right or wrong answer to this decision-making process, the DMs can be aided with adequate problem-related information with an easy-to-understand visualization tool to make a proper choice. A recent study (Nagar et al., 2021) by the author group has shown that an interpretable version of self-organizing maps (they named the procedure as 'iSOM') can produce a series of two-dimensional SOM plots of each objective and constraint function in two fictitious mapped axes of the entire n -dimensional search space. The SOM plots are called the component planes of the respective variables, objectives, or constraints. The objective/constraint values are shown in small hexagonal (or rectangular) colored cells indicating their values. Since the axes are kept invariant for each objective/constraint SOM plot, a good idea of the trade-off among objectives can be perceived by traversing in certain fixed directions on two or more SOM plots. Moreover, the SOM plots provide a clear direction of maximal increase and decrease of each function value, thereby allowing one to investigate the change in other function values along the fixed directions to get a good idea of trade-off among objectives and constraints.

In this paper, we take the NIMBUS start point and show it on iSOM component planes to provide a clear understanding of the start point in the entire search space. This allows the DMs to have a better understanding of trade-off of objectives and constraints, so they are in a more informed position to provide classification levels of objectives and visualize the part of Pareto front obeying the classification, which is the region of interest (RoI) as well. iSOM visualization aids to select alternate solutions, generate intermediate solutions, and choose the final solution, knowing fully the scope of feasible solutions and RoI. In addition, the DMs are provided with the previous iteration's NIMBUS solutions on the same iSOM component planes to have a clear idea of their relative importance to progress to the next iteration. Since the iSOM procedure is agnostic to the actual variable space dimension and plots are always shown in two dimensions, they are relatively easy to comprehend. Moreover, our proposed iSOM component planes use different innovative fills and colors of hexagonal cells to make the whole process attractive and easier to use, a matter which is not possible to achieve with existing visualization methods. The major contributions of the current work are as follows:

1. Integrating an inherently interpretable visualization technique, iSOM with NIMBUS for interactive MCDM leading to a better comprehension of the various properties of the preferred solutions.
2. Identify disjoint regions in the Pareto front from the U-matrix of iSOM.
3. Along with the objective function values, the properties of the solutions such as their proximity to the constraint and trade-off information are used as a criterion for the MCDM task leading to better decisions.
4. The ability of iSOM in permitting the DM to provide preference information for various steps such as classification, selecting alternate solution(s), and final solution of NIMBUS method for informed decision-making.

In the remainder of this paper, we provide a brief description of the NIMBUS method in a step-by-step format in Section 2 and emphasize the need for using an effective visualization method to accompany its iterative steps. Then in Section 3, we provide a brief description of the iSOM procedure. The overall procedure of iSOM-based visualization for NIMBUS method is provided in step-by-step format with details of color and style coding in Section 4. The advantages of using the iSOM-NIMBUS procedure compared to existing methods are highlighted in Section 5 in the context of a real-world three-objective crash-worthiness problem. Thereafter, the iSOM-NIMBUS procedure is further applied to different benchmark problems (five-objective problem, disjointed Pareto-set problem, and constrained problem) in Section 6. Finally, iSOM-NIMBUS is applied to two more real-world problems in Section 7. Conclusions of this extensive study is then summarized in Section 8.

2. NIMBUS Algorithm

NIMBUS refers to Non-differentiable Interactive Multiobjective BUNDLE-based optimization System. As the name suggests, it is a multiobjective optimization (MOO) system that is able to handle even non-differentiable functions (Miettinen et al., 2008; Miettinen and Mäkelä, 1999). However, the assumptions behind the implementation of NIMBUS are that all objective functions and constraint functions are locally Lipschitz continuous and that the feasible region $\{\mathbf{x} \in \mathbb{R}^n \mid \mathbf{g}(\mathbf{x}) \leq 0\}$ is convex (Miettinen and Mäkelä, 1996) (\mathbf{x} is the vector of the design variable and $\mathbf{g}(\mathbf{x})$ is the set of constraints functions). Given the MOO problem:

$$\begin{aligned} & \underset{(\mathbf{x})}{\text{Minimize}} \quad \{f_1(\mathbf{x}), \dots, f_M(\mathbf{x})\}, \\ & \text{subject to:} \quad \mathbf{g}(\mathbf{x}) = (g_1(\mathbf{x}), \dots, g_J(\mathbf{x}))^T \leq 0, \end{aligned} \quad (1)$$

where $\mathbf{f}(\mathbf{x}) = \{f_1(\mathbf{x}), \dots, f_M(\mathbf{x})\}^T$ is a vector of objective functions. NIMBUS is based on the classification of the objective functions f_i into the following five classes (Miettinen and Mäkelä, 1999), based on the objective vector $\mathbf{f}(\mathbf{x}^h)$ at the current solution \mathbf{x}^h , as follows:

1. whose values should be minimized further requiring $f_i(\mathbf{x}) < f_i(\mathbf{x}^h)$, for $i \in I^<$,
2. whose values should be minimized till some aspiration level $\bar{z}_i (< f_i(\mathbf{x}^h))$, such that $f_i(\mathbf{x}) \geq \bar{z}_i$ for $i \in I^{\leq}$,
3. whose current values are satisfactory at the moment ($i \in I^=$),
4. whose values are allowed to increase until or up to a specific upper bound $\epsilon_i (\geq f_i(\mathbf{x}^h))$, such that $f_i(\mathbf{x}) \leq \epsilon_i$ for $i \in I^{\geq}$, and
5. whose values can change freely ($i \in I^{>}$).

The difference between the classes $I^<$ and I^{\leq} is that the functions in the former class are to be minimized as far as possible, as the functions in the latter class are to be minimized only till the aspiration level. At each iteration, the DM has the option to classify the objective functions at a feasible start point/current solution. Based on the classification a new (multiobjective) optimization problem is formed and solved by *Multiobjective Proximal Bundle* (MPB) method (Miettinen and Mäkelä, 1996).

The authors of the NIMBUS method have changed the formulation of the scalarization problem many times since their first study (Miettinen and Mäkelä, 2006), but the one shown below (Miettinen and Mäkelä, 2002) guarantees finding a Pareto-optimal solution. Let $\mathbf{f}(\mathbf{x}^h)$ be the feasible start point at an iteration, at which the classification is performed. Further to the classification, the following augmented achievement scalarizing function (AASF) sub-problem is formulated:

$$\begin{aligned} & \underset{(\mathbf{x})}{\text{Minimize}} \quad \max_{i \in I^<, j \in I^{\leq}} \left[\frac{f_i(\mathbf{x}) - z_i^*}{z_i^{\text{nad}} - z_i^{**}}, \frac{f_j(\mathbf{x}) - \bar{z}_j}{z_j^{\text{nad}} - z_j^{**}} \right] + \rho \sum_{i=1}^M \frac{f_i(\mathbf{x})}{z_i^{\text{nad}} - z_i^{**}}, \\ & \text{subject to:} \quad f_i(\mathbf{x}) \leq f_i(\mathbf{x}^h), \quad i \in I^< \cup I^{\leq} \cup I^=, \\ & \quad \quad \quad f_i(\mathbf{x}) \leq \epsilon_i, \quad i \in I^{\geq}, \\ & \quad \quad \quad \mathbf{g}(\mathbf{x}) = (g_1(\mathbf{x}), \dots, g_J(\mathbf{x}))^T \leq 0, \end{aligned} \quad (2)$$

where, z_i^{nad} and z_i^* are nadir and ideal objective values, respectively, of the i -th objective, and z_i^{**} (slightly smaller than z_i^*) is the Utopian objective value. These values are computed at the start of the NIMBUS procedure. While it

is possible to obtain the ideal objective vector by minimizing each constrained objective function individually, the nadir objective vector can only be estimated (Deb and Miettinen, 2010). The parameter ρ (>0) is usually chosen to be a small scalar value and the term including ρ ensures that the resulting optimal solution of the above problem is a Pareto-optimal point, and not a weak Pareto-optimal point (Miettinen, 2012). The denominators in the terms of the objective function control the reference direction for the AASF formulation.

Miettinen and Mäkelä (1996) also proposed the use of the following three more sub-problem formulations to find *alternate* solutions using other standard MCDM approaches. In the next sub-problem, the scalarizing function used is STOM (Nakayama and Sawaragi, 1984):

$$\begin{aligned} \text{Minimize}_{(\mathbf{x})} \quad & \max_{i=1, \dots, M} \left[\frac{f_i(\mathbf{x}) - z_i^{**}}{\bar{z}_i - z_i^{**}} \right] + \rho \sum_{i=1}^M \frac{f_i(\mathbf{x})}{\bar{z}_i - z_i^{**}} \\ \text{subject to:} \quad & \mathbf{g}(\mathbf{x}) = (g_1(\mathbf{x}), \dots, g_J(\mathbf{x}))^T \leq 0. \end{aligned} \quad (3)$$

For objectives not belonging to I^{\leq} class, \bar{z}_i is set to z_i^* . The denominator of the terms in the objective function is different, thereby causing a different reference direction for the resulting AASF problem. Notice that no additional constraint is used in this formulation, thereby ignoring ε_i information. The resulting solution may not satisfy $f_i(\mathbf{x}) \leq f_i(\mathbf{x}^h)$ constraint for $i \in I^< \cup I^{\leq} \cup I^=$ and $f_i(\mathbf{x}) \leq \varepsilon_i$ for $i \in I^{\geq}$.

In the third sub-problem formulation, the scalarizing function used, comes from the reference point method (Deb and Jain, 2014):

$$\begin{aligned} \text{Minimize}_{(\mathbf{x})} \quad & \max_{i=1, \dots, M} \left[\frac{f_i(\mathbf{x}) - z_i^{**}}{z_i^{\text{nad}} - z_i^{**}} \right] + \rho \sum_{i=1}^M \frac{f_i(\mathbf{x})}{z_i^{\text{nad}} - z_i^{**}} \\ \text{subject to:} \quad & \mathbf{g}(\mathbf{x}) = (g_1(\mathbf{x}), \dots, g_J(\mathbf{x}))^T \leq 0. \end{aligned} \quad (4)$$

This formulation does not use \bar{z}_i or ε_i information.

The scalarizing function used in the fourth sub-problem formulation to be introduced is related to the one used in the GUESS method (Buchanan, 1997):

$$\begin{aligned} \text{Minimize}_{(\mathbf{x})} \quad & \max_{i=1, \dots, M} \left[\frac{f_i(\mathbf{x}) - z_i^{\text{nad}}}{z_i^{\text{nad}} - \bar{z}_i} \right] + \rho \sum_{i=1}^M \frac{f_i(\mathbf{x})}{z_i^{\text{nad}} - \bar{z}_i} \\ \text{subject to:} \quad & \mathbf{g}(\mathbf{x}) = (g_1(\mathbf{x}), \dots, g_J(\mathbf{x}))^T \leq 0. \end{aligned} \quad (5)$$

For objectives not in the I^{\leq} class, \bar{z}_i is set to z_i^* .

On solving the scalarized MOO problems (2), (3), (4) and (5), the solutions obtained are referred to as alternate solutions. If a specific alternate solution is not desirable, a number of intermediate points can be examined between two alternate solutions on a line joining them. In the last step, the Pareto-optimality of the final solution is guaranteed by solving the following additional problem with slack variables γ_i :

$$\begin{aligned} \text{Maximize}_{(\mathbf{x}, \gamma)} \quad & \sum_{i=1}^M \gamma_i, \\ \text{subject to:} \quad & f_i(\mathbf{x}) + \gamma_i \leq f_i(\mathbf{x}^h), \quad i \in I^<, \\ & \gamma_i \geq 0, \quad i \in I^<, \\ & \mathbf{g}(\mathbf{x}) = (g_1(\mathbf{x}), \dots, g_J(\mathbf{x}))^T \leq 0. \end{aligned} \quad (6)$$

If the solution to the above problem is equal to $(\mathbf{x}^h, \mathbf{0})$, then \mathbf{x}^h is guaranteed to be Pareto-optimal and is appointed as the final solution. Finally, the solution process stops once the aspiration level of the DMs is obtained.

NIMBUS is a flexible method where the DMs can proceed in several ways by providing information about the aspiration level in each iteration of the algorithm. The overall NIMBUS algorithm is provided below in item-by-item format with a mention of steps in which iSOM can be employed for a better understanding:

1. Given the MOO problem (1), find ideal point (\mathbf{z}^*) and estimate nadir point (\mathbf{z}^{nad}) using the pay-off table or other methods (Miettinen, 2012), or from a representative set of EMO solutions. Set an Utopian point $\mathbf{z}^{**} = \mathbf{z}^* - \epsilon$ (usually, $\epsilon_i = 10^{-3}$).
2. Choose a feasible starting point \mathbf{x}^0 and calculate a Pareto-optimal solution \mathbf{x}^1 as a *start point*, with $I^< = \{1, \dots, M\}$. Set $h = 1$.

3. Divide the objective functions into *five classes* $I^<, I^{\leq}, I^=, I^{\geq},$ and $I^{>}$ at the point $\mathbf{f}(\mathbf{x}^h)$ such that $I^{\geq} \cup I^{>} \neq \emptyset$ and $I^{<} \cup I^{\leq} \neq \emptyset$. They ensure that an improvement in an objective must come from a deterioration on at least one other objective. If either of the unions is empty, go to Item 10. Obtain the *aspiration levels* \bar{z}_i^h for $i \in I^{\leq}$ and the *upper bounds* ϵ_i^h for $i \in I^{\geq}$ from the DM. (iSOM-aided)
4. Find at most four alternate solutions $\hat{\mathbf{x}}^{h,k}$ by solving each of the k -th sub-problems defined in (2), (3), (4) and (5) by the MPB routine. If $\hat{\mathbf{x}}^{h,k} = \mathbf{x}^h$ for all k , ask the DM whether (s)he wants to try *another classification*. If yes, set $\mathbf{x}^{h+1} = \mathbf{x}^h$, $h = h + 1$, and go to Item 3 for finding new set of *alternate solutions*. If no further classification is desired, go to Item 10. If $\hat{\mathbf{x}}^{h,k} \neq \mathbf{x}^h$ for any k , $\hat{\mathbf{x}}^{h,k}$ is an alternate solution. Go to Item 5 with all alternate solutions. (iSOM-aided)
5. Present $\mathbf{f}(\mathbf{x}^h)$ and all $\mathbf{f}(\hat{\mathbf{x}}^{h,k})$ to the DM. If the DM does not like any of the alternate solutions and *prefers* $\mathbf{f}(\mathbf{x}^h)$, set $\mathbf{x}^{h+1} = \mathbf{x}^h$, $h = h + 1$, and to go Item 3 for a different classification process. Otherwise, if the DM prefers a specific alternative solution $\hat{\mathbf{x}}^{h,\bar{k}}$ more than other solutions, go to Item 6. Otherwise (the DM likes more than one solution in the set $(\mathbf{x}^h, \hat{\mathbf{x}}^{h,k})$), the DM chooses two most preferred solutions out of the set $(\mathbf{x}^h, \hat{\mathbf{x}}^{h,k})$. Let us say that the two chosen solutions are \mathbf{x}^A and \mathbf{x}^B . Set $\mathbf{d}^h = \mathbf{x}^A - \mathbf{x}^B$ and go to Item 7. (iSOM-aided)
6. At this step, the DM wants to continue from $\mathbf{f}(\hat{\mathbf{x}}^{h,\bar{k}})$. If $I^{<} \neq \emptyset$, set $\mathbf{x}^{h+1} = \hat{\mathbf{x}}^{h,\bar{k}}$, $h = h + 1$, and to go Item 3 for finding a new set of alternate solutions arising from $\hat{\mathbf{x}}^{h,\bar{k}}$. Otherwise ($I^{<} = \emptyset$), the Pareto-optimality of $\hat{\mathbf{x}}^{h,\bar{k}}$ must be checked by setting $I^{<} = \{1, \dots, M\}$ and employing the MPB method to solve the resulting problem (6). Let the solution be $\hat{\mathbf{x}}^h$ and set $\mathbf{x}^{h+1} = \hat{\mathbf{x}}^h$. Set $h = h + 1$, and go to Item 3. (iSOM-aided)
7. Compute P different criterion vectors uniformly $\mathbf{f}(\mathbf{x}^A + t_j \mathbf{d}^h)$, where $t_j = \frac{j-1}{P-1}$, $j = 1, \dots, P$.
8. Produce P *intermediate* Pareto-optimal solutions $\bar{\mathbf{x}}^h$ from the computed criterion vectors employing the MPB method (with $I^{<} = \{1, \dots, M\}$). Store all alternate solutions and intermediate solutions in a database D .
9. Present P intermediate criterion vectors to the DM and let the DM choose the *most preferred one* among them. Denote the corresponding solution by \mathbf{x}^{h+1} . Set $h = h + 1$. If DM further wants to generate P intermediate solutions between the two intermediate solutions \mathbf{x}^A and \mathbf{x}^B , then go to Item 7. If the DM wants to continue to improve solutions, go to Item 3, otherwise, go to Item 10. (iSOM-aided)
10. Check the Pareto-optimality of \mathbf{x}^h by solving the problem (6). Let the solution be $(\tilde{\mathbf{x}}, \tilde{\gamma})$. If $\tilde{\mathbf{x}} = \mathbf{x}^h$, the final solution is $\tilde{\mathbf{x}}$, otherwise, go to Item 3, by setting $\mathbf{x}^h = \tilde{\mathbf{x}}$.

If the solution of the problem (6) is equal to $(\mathbf{x}^h, \mathbf{0})$, then \mathbf{x}^h is guaranteed to be Pareto optimal and can be appointed as the final solution. If \mathbf{x}^h is not Pareto-optimal, then $\hat{\mathbf{x}}$ is Pareto-optimal solution.

Note that the DM can be aided with an easy-to-use visualization method in arriving at a decision at all italicized tasks in Items 2, 3, 4, 7, and 9 to (i) Define Start point, (ii) provide a classification of objectives, and set aspiration and upper bounds, (iii) seek different alternate solutions if needed, (iv) generate intermediate solutions and (v) choose the most preferred out of P intermediate solutions or from database D . NIMBUS employs a few standard visualization techniques for DM to facilitate decision-making: (i) Bar chart technique (ii) Petal diagram technique, and (iii) Value path (or parallel coordinate plot (PCP)) technique. The applicability of bar chart and petal diagrams are limited only to a few solutions. For handling a large number of alternate solutions and intermediate solutions, it is often difficult to visualize and compare each solution with these methods. With value path visualization, although one can visualize a large number of solutions, it is difficult to get a clear idea of the trade-off information or infer disjoint, holes, closeness to constraint boundaries, nearness to other chosen solutions, or other features of the solutions, which would be crucial in making the above decisions. In this study, we propose the use of iSOM (described in the next section) to visualize NIMBUS solutions, such as the start point, alternate solutions, intermediate solutions, and, of course, the final solution. In addition, iSOM also permits visualizing NIMBUS solutions near the boundary of the Pareto-optimal front, near disjointed regions or holes, near-constraint solutions, and, importantly, the current location of the solutions in the front along with a clear idea of the extent of the unexplored and explored parts of the Pareto-optimal front for a continuation of the NIMBUS method. We shall demonstrate the use of iSOM in NIMBUS method through several examples in Sections 5 to 7.

3. Brief Introduction to Self-Organizing Map (SOM)

Self-organizing maps (SOM) is a type of Artificial Neural Network (ANN) that is based on unsupervised learning. It takes high-dimensional data (each with n variables and one response) $\mathbf{v} = [\mathbf{x}_1, \mathbf{x}_2, \dots, \mathbf{x}_n, \mathbf{y}]$ as input and maps them into a low-dimensional space, generally, a two-dimensional representation of the input data. This two-dimensional representation consists of nodes, which are connected in a rectangular or a hexagonal grid to form a 'Map'. Each node (say j^{th}) is associated with the weight vector $\mathbf{w}_j = [m_1^j, m_2^j, \dots, m_n^j, m_y^j]$ such that the dimension of the weight vector is equal to the dimension of data set. Each dimension i.e. input and response is represented by a 2-d map on a color scale called the component plane. The color scale on the component planes represents the variation and interaction between the input and response. A schematic of the self-organizing map depicting its working principle is presented in Fig. 1. Training of SOM includes finding out the Best Matching Units (BMUs) and a weight update rule. It also preserves the topology of the high-dimensional input space into the low-dimensional space.

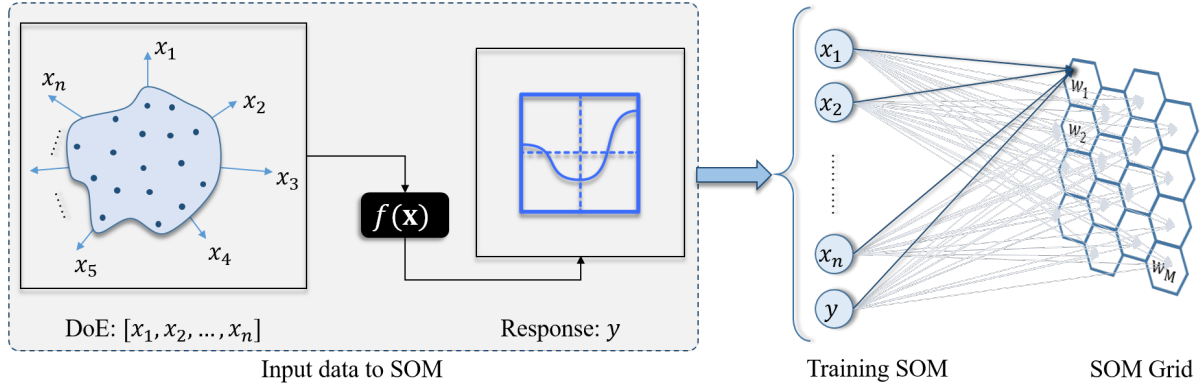


Figure 1: Working principle of Self-Organizing Map. Input data points are used to construct a mapping on a two-dimensional uniform grid.

3.1. Conventional Self-Organizing Map (cSOM)

Neurons of SOM are called nodes that form a hexagonal or rectangular grid (Kohonen, 1997). Each node is associated or assigned with a weight vector that is called a code-book vector whose dimension is equal to the high dimensional data as presented in Fig. 1. SOM algorithm consists of two steps first initialization followed by training as the second step. During the initialization, SOM assigns some initial weights to nodes.

The initial weights i.e. code-book can be chosen randomly or linearly from the data set. If initial weights are chosen randomly it is called random initialization and if chosen as a linear combination of a given data set then called linear initialization. The training step includes Best matching Unit (BMU) calculation based on the Euclidean distance and weight update rule iteratively in order to map the high dimensional data into a 2-dimensional representation. During the BMU calculation step, a data point is assigned as the winner node for which the SOM node has the minimum Euclidean distance. In the training step, the weight of the BMUs is updated in order to map the shape and topography of the given high-dimensional data set.

Training in a conventional SOM (cSOM) algorithm consists of choosing a winner node called the Best Matching Unit (BMU). The BMU is a node that has the least distance from the selected data point in the n -dimensional input space. Upon identifying the BMU, the weight vector of the respective node and nodes in its neighborhood are modified based on the weight update rule.

Assume that the given data-set consists of n -dimension in input $[x_1^i, \dots, x_n^i]$ and a single response y^i , where $i = 1, \dots, N$. In order to map the given data-set the input to SOM will be a $(n+1)$ -dimensional data-set $\mathbf{v}^i = [x_1^i, \dots, x_n^i, y^i]_{i=1}^N$; the M SOM node's weights can be expressed as $\mathbf{w}^j = [m_1^j, \dots, m_n^j, m_y^j]_{j=1}^M$. BMU calculation and weight update is performed during the iterative training process. The governing equation for the BMU calculation is-

$$c_i = \underset{j=1}{\operatorname{argmin}} \{ ||\mathbf{v}^i - \mathbf{w}^j|| \}; \quad i = 1, \dots, N. \quad (7)$$

Upon identifying the BMUs the weight update of the j -th winner node and its neighboring nodes take place as per the equation (8).

$$\mathbf{w}^j(t+1) = \mathbf{w}^j(t) + \Phi(c_i, j, t) \times L(t) \times (\mathbf{v}^i - \mathbf{w}^j(t)). \quad (8)$$

Φ is the neighbourhood function around the winner node \mathbf{w}^{c_i} for the j -th node at t -th iteration for the i -th input vector and $L(t)$ is Learning rate.

The neighborhood function (Φ) and associated Equations are presented in (9).

$$\begin{aligned} \Phi(c_i, j, s) &= \exp\left(-\frac{\|\mathbf{w}^{c_i} - \mathbf{w}^j\|^2}{2\sigma(s)^2}\right), \\ \sigma(s) &= \sigma_0 - \frac{(s-1)\sigma_0}{N \times t_{max} - 1}, \\ s(t) &= (t-1) \times N + 1, \end{aligned} \quad (9)$$

where s is the update step, t is the iteration number, σ_0 is the initial radius that takes the default value as 1 and decays linearly with the iteration (t) as presented in (10).

$$\begin{aligned} L(s) &= C \times \frac{\alpha_0}{C + s}, \\ C &= \frac{N}{100}, \end{aligned} \quad (10)$$

where α_0 is a hyperparameter that takes a default value of 0.5 and C is a constant. The reader is referred to Kohonen (1997) for additional details about cSOM.

This method of initialization and training is done in conventional Self-Organising Maps (cSOM) that suffer from self-intersection and folding of the map grid resulting in loss of topography and trend of the response which affects the visualization. To overcome these issues, interpretable Self Organizing Map (iSOM) was introduced (Thole and Ramu, 2020).

3.2. Interpretable Self-Organizing Map (iSOM)

Thole and Ramu (2020) suggested a different BMU finding and weight update rule to avoid the folding and self-intersection of cSOM. Topology preservation and avoidance of the self-intersection are two key features that make iSOM better than cSOM. In iSOM, the BMU is calculated by using the input vector only, whereas the weight update rule during training considers the response only. This modification provides the interpretability between the input space and response, hence termed as interpretable Self-Organizing Maps (iSOM). iSOM performs linear initialization on the data set whereas BMU finding takes place in input space in the training phase and weight update is performed in response only. The modification proposed during the training is given in the below set of eqns. (11)-

$$\begin{aligned} m_i^j(t+1) &= m_i^j(t), \quad i = 1, \dots, n, \\ m_y^j(t+1) &= m_y^j(t) + \Phi(c_i, j, t) \times L(t) \times (y^i - m_y^j(t)). \end{aligned} \quad (11)$$

The modification suggested in the eq. (11) during the training process avoids the self-intersection and folding of the SOM grid and allows interpretable visualization and exploration of design space by preserving the topography of the response with respect to the input space. This ability of iSOM to preserve the topography allows the DM to visualize and interpret the functional relation between the input space and response. Further details on iSOM are documented in Thole and Ramu (2020) which discusses the interpretability of iSOM in the context of design space exploration. In the current work, we use iSOM to visualize and interpret the interaction between the objective functions to aid the DMs in the MCDM task. A recent study (Nagar et al., 2021) has compared cSOM and iSOM in the context of visualizing multi-criterion Pareto-optimal solutions and demonstrated the advantage of iSOM on several standard and real-world problems. We are now ready to discuss how the iSOM visualization method can be applied to make the NIMBUS application easier and more convenient for DMs.

4. Proposed iSOM-based Visualization within NIMBUS Method

Nagar et al. (2021) proposed the use of iSOM to visualize the Pareto-optimal front. In the current work, we extend iSOM's capabilities for convenient visualization of NIMBUS solutions, as discussed below. NIMBUS finds different

solutions in different steps during the iterative process. Hence, it is essential to distinguish those solutions and select the preferred solution based on their properties and relative positions in the Pareto optimal front. The following subsections address the different NIMBUS solutions, their relative position in Pareto optimal front, and provide a unique color code scheme to iSOM nodes.

4.1. Identifying Boundary Points of Pareto Disjoint Regions

The boundary points of the Pareto disjoint region are identified from the unified distance matrix (U matrix) of the iSOM component planes of the objective functions. U-matrix is a 2-D map that plots the distance between two neighboring nodes/cells in an intermediate node (Kohonen, 1997). Larger values of the intermediate nodes in the U-matrix represent the disjoint region in the Pareto optimal front. The nodes/cells of the component planes of the objective function corresponding to the larger value in the U-matrix are identified and plotted using the color code defined in Table 1.

4.2. Visualization of Trade-offs among the Objectives

Often DM wishes to select one or many the preferred solutions based on the trade-off values of objectives. We propose plotting a separate iSOM component plane ($T(\mathbf{x})$) indicating the trade-offs of objectives, for convenient visualization. The trade-off metric $T(\mathbf{x}^i)$ for a Pareto-optimal solution \mathbf{x}^i in the objective space is computed as follows

$$T(\mathbf{x}^i) = \frac{|B(\mathbf{f}(\mathbf{x}^i))|}{\max_{j=1} \theta(\mathbf{x}^i, \mathbf{x}^j)}, \quad (12)$$

in a defined neighborhood $B(\mathbf{f}(\mathbf{x}^i))$. The neighborhood of the solution $\mathbf{f}(\mathbf{x}^i)$ has been computed in Pareto front (objective function) space using the euclidean distance. $B(\mathbf{f}(\mathbf{x}^i))$ is the neighbourhood solutions in the vicinity of the solution \mathbf{x}^i in objective function space. The number of neighborhoods i.e. $|B(\mathbf{f}(\mathbf{x}^i))|$ is usually decided by the DM. Here, $\theta(\mathbf{x}^i, \mathbf{x}^j)$ is the trade-off between two neighboring solutions \mathbf{x}^i and \mathbf{x}^j , defined as the ratio of the average loss in objective values to the average gain in objective values for moving from \mathbf{x}^i to \mathbf{x}^j :

$$\theta(\mathbf{x}^i, \mathbf{x}^j) = \frac{\bar{L}(\mathbf{x}^i, \mathbf{x}^j)}{\bar{G}(\mathbf{x}^i, \mathbf{x}^j)}. \quad (13)$$

The average loss and gain functions are defined below:

$$\bar{L}(\mathbf{x}^i, \mathbf{x}^j) = \frac{\sum_{k=1}^M \max(0, f_k(\mathbf{x}^j) - f_k(\mathbf{x}^i))}{\sum_{k=1}^M \{ \mathbb{1} [f_k(\mathbf{x}^j) > f_k(\mathbf{x}^i)] \}}, \quad (14)$$

$$\bar{G}(\mathbf{x}^i, \mathbf{x}^j) = \frac{\sum_{k=1}^M \max(0, f_k(\mathbf{x}^i) - f_k(\mathbf{x}^j))}{\sum_{k=1}^M \{ \mathbb{1} [f_k(\mathbf{x}^i) > f_k(\mathbf{x}^j)] \}}. \quad (15)$$

Here, $\{ \mathbb{1} [f_k(\mathbf{x}^j) > f_k(\mathbf{x}^i)] \}$ denotes the count for which the criteria defined in $[.]$ holds true. The term inside the indicator function checks the condition for which the current solution (\mathbf{x}^i) is better than the neighboring solution (\mathbf{x}^j) in the k^{th} objective function f_k . It is to be noted that $j = 1, \dots, |B(\mathbf{f}(\mathbf{x}^i))|$. M is the number of objective functions. After $T(\mathbf{x}^i)$ is computed for each Pareto solution, these values can be used to plot iSOM component planes of trade-offs (T) that will be convenient for DM in selecting the preferred solution in MCDM task. Visualizing iSOM component plane of trade-offs (T) DM may wish to select solutions corresponding to the higher values of T .









4.3. Identifying Near-Constraint Points

In order to visualize the Pareto-optimal solutions near the constraint boundary, the average of the normalized constraint value $G(\mathbf{x})$ is trained and plotted on a separate component plane G using iSOM. It is to be noted that G is only computed on the feasible solutions at which there is no constraint violation. The values for generating the component plane G can be computed as follows:

$$G(\mathbf{x}) = \frac{1}{J} \sum_{j=1}^J \hat{g}_j(\mathbf{x}) [\mathbb{1} (\hat{g}_j(\mathbf{x}) < 0)], \quad (16)$$

Table 1

Color code for visualization using iSOM for distinguishing the different NIMBUS solutions and selecting the preferred solution based on their properties and relative positions in Pareto optimal front. Edge (edge of iSOM node), Face (Face of iSOM node), Color (Edge color/ Face color of corresponding iSOM node), Node (for demonstration purpose).

S.No.	Points	Edge	Face	Color	Node
1	Boundary points	Yes	No	Black	
2	Near-constraint points	No	Yes	Grey	
3	Start point/ current solution	No	Yes	Black	
4	Selected points after classification	Yes	No	White	
5	Un-selected points in respective objectives after classification	Yes	No	Red	
6	Alternative solutions	No	Yes	Magenta	
7	Intermediate solutions	No	Yes	Green	
8	Final solution	No	Yes	Red	

where, $\hat{g}_j(\mathbf{x})$ is the j -th normalized constraint function (Deb, 2011) of $g_j(\mathbf{x}) - b_j \leq 0$ (b_j being the resource value of a typical constraint) obtained as $\hat{g}_j(\mathbf{x}) = g_j(\mathbf{x})/b_j - 1 \leq 0$, and J is the number of constraints. Let us say that the number of feasible solutions are $n_f = |G(\mathbf{x})|$. In order to indicate the near-constraint points, we identify top 10% ($n_G = \lceil 0.1 \times n_f \rceil$) feasible solutions (\mathbf{x}_G^k , for $k = 1, \dots, n_G$) close to the constraint boundaries by first sorting the points in descending order of G and picking the top 10% of points from the sorted list.

Then, respective cells (\mathbf{c}_G^k , for $k = 1, \dots, n_G$) are found by finding the closest cell in the G component plane to each of the \mathbf{x}_G^k solutions. These cells are plotted on each component plane using the color code defined in Table 1 (S.No. 2).

4.4. Selected Search Space after Classification

Every classification made in Item 3 of the NIMBUS method can provide the DMs an idea of selected and un-selected parts of the search space that can be visualized on iSOM component plane of objectives. For the current solution \mathbf{x}^h , all Pareto optimal points that conform to the classification of objectives, provided by the DMs, can be identified and marked on the respective iSOM component plane of objectives. They represent the selected Pareto points for the current iteration. Such a visual check can allow the DMs to make a final consideration in leaving Item 3. In addition, the cells that do not conform to the provided classification of objectives can be marked in a different color and style to indicate the opposite. The respective color code scheme for both selected and un-selected search regions are shown in Table 1 (S.No. 4 and 5).

4.5. NIMBUS Points

Every iteration of the NIMBUS method begins with several key points: (i) current point (\mathbf{x}^h) (or, a user-specified start-point \mathbf{x}^0) in Item 2, (ii) a derived MPB solution $\hat{\mathbf{x}}^h$ in Item 4, and (iii) several created intermediate points $\bar{\mathbf{x}}^h$ in Item 7, of which the most preferred solution is chosen in Item 9. In addition to visualizing these solutions using iSOM component planes for a better understanding of the NIMBUS method, another important solution to include in the visualization process is the final point ($\bar{\mathbf{x}}$) of the overall NIMBUS method. The respective iSOM cells can be marked differently for each of the above points (described in Table 1- S.No. 6 to 8) to have a better comprehension of the progress of NIMBUS method.

4.6. Augmentation of NIMBUS with Focused EMO Algorithm

In the event of fewer points in the vicinity of intermediate solutions in Item 8, a focused EMO algorithm, such as R-NSGA-II (Deb and Sundar, 2006) or R-NSGA-III (Vesikar et al., 2018) or other methods can be employed. These methods use a population-based evolutionary multi-objective optimization method to find multiple trade-off solutions

in a focused region on the Pareto-optimal front dictated by a DM-supplied reference point \mathbf{z}^r and a shrinkage factor (μ). In this study, we choose them as follows:

$$\mathbf{z}^r = \frac{\mathbf{F}^{alt1} + \mathbf{F}^{alt2}}{2}, \quad (17)$$

$$\mu = \max_{i=1}^M \left[\frac{|f_i^{alt1} - f_i^{alt2}|}{f_i^{\max} - f_i^{\min}} \right]. \quad (18)$$

where, \mathbf{F}^{alt1} and \mathbf{F}^{alt2} are two alternate MPB solutions and f_i^{\min} and f_i^{\max} are the minimum and maximum values of i -th objective function. Focused EMO approaches create a set of well-distributed reference points on a unit simplex close to \mathbf{z}^r and then shrink the points by μ to make them closer to each other. Thereafter, a reference point-based EMO procedure, such as NSGA-III (Deb and Jain, 2014), is applied to find respective focused Pareto-optimal points close to the alternate solutions. After generating the focused solutions, DM can plot them in iSOMs on the objective function space and visualize the preferred solution only, instead of on the complete Pareto-optimal front. The visualization of NIMBUS solution on the component plane of preferred solutions allows a larger spread as compared to the component plane of the complete Pareto optimal solution. Thus, visualization of NIMBUS solutions on the component plane of preferred solutions can also be referred to as *local visualization using EMO*.

4.7. Proposed iSOM-aided NIMBUS method

The steps of iSOM-aided NIMBUS are discussed below:

- Step 1:** Obtain a set of complete Pareto optimal front for the given MOO using an EMO procedure.
- Step 2:** Plot the iSOM component plane for each objective and constraint function using Pareto-optimal points after Item 1 of the NIMBUS method.
- Step 3:** Identify the Pareto disjoint regions using the U-matrix and plot them on the iSOM component planes according to the color code defined in Table 1.
- Step 4:** Plot near-constraint points on the component plane of objective functions and the average of normalized constraint violation component plane G .
- Step 5:** Select the start point or current point on iSOM component planes. (Item 2 in NIMBUS algorithm)
- Step 6:** At the start point or current point, define the NIMBUS classification according to the desired aspiration/upper level and visualize selected and un-selected Pareto regions on the iSOM component planes of objectives. (Item 3 in NIMBUS algorithm)
- Step 7:** Obtain and plot alternate solutions on iSOM component plane. (Item 4 in NIMBUS algorithm)
- Step 8:** If DM wants to further classify the objective functions at an alternate solution, go to Step 6, otherwise select two alternate solutions aided by iSOM visualization. (Items 5 and 6 in NIMBUS algorithm)
- Step 9:** Generate intermediate solutions between two alternate solutions (if DM wants to explore more points) and plot it using iSOM, go to Step 11. (Item 7 in NIMBUS algorithm)
- Step 10:** If DM wants to visualize solutions locally, generate focused EMO solutions by R-EMO algorithm using Equations (17) and (18) and visualize locally.
- Step 11:** If aspiration level is attained, select the final solution and mark it on the iSOM component plane; otherwise go to Step 8. (Items 9 and 10 in NIMBUS algorithm)

A flowchart of the main steps is provided in the supplementary document.

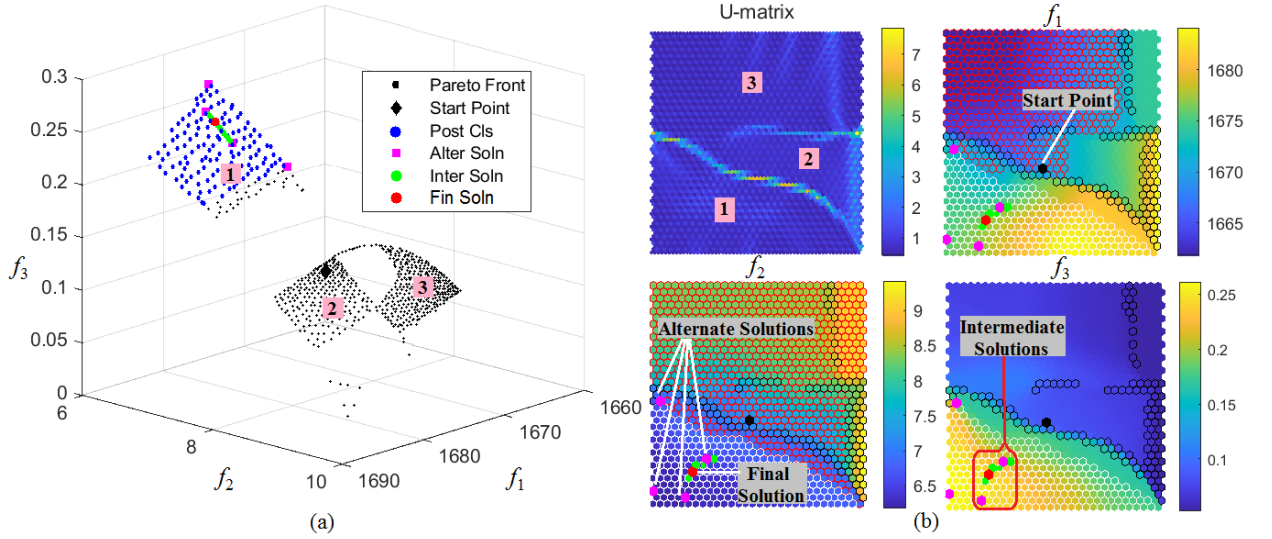


Figure 2: Crash worthiness problem: (a) Scatter Plot of NSGA-III-obtained Pareto solutions are marked with NIMBUS solutions, blue markers depict search space selected after classification, (b) U-matrix plot indicates Pareto boundary cells having relatively large values of U , indicating three clear clusters that exist on the obtained Pareto front. f_1 , f_2 and f_3 are component plane of objective functions, for which each cell indicates the respective f_i values. Cells with black edge color depict Pareto disjoint boundary inferred from the U-matrix. The cells with red and white edge colors represent objective-wise un-selected points and selected points respectively after classification. The cells with black face color represent the start point, magenta face color represents alternate solutions, green face color represents intermediate solutions, and red face color represents the final solution. The color code scheme is provided in Table 1.

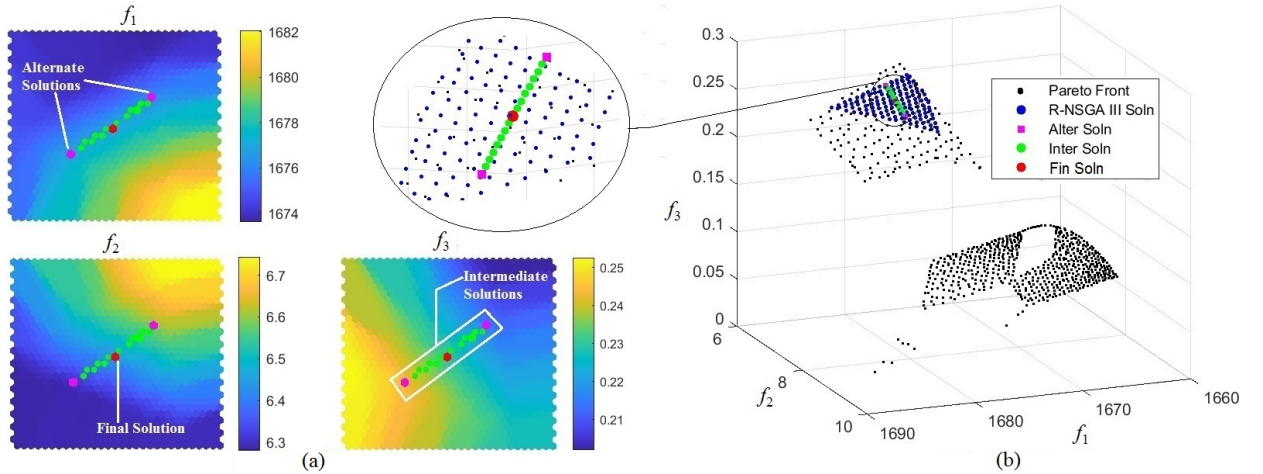


Figure 3: Crash-worthiness problem: (a) iSOM component plane of objectives, (b) Scatter plot of R-NSGA-III points in the context of the entire Pareto-optimal front. The region of interest is blown up for clarity. The use of focused R-NSGA-III iSOM component planes allows a more convenient decision-making approach.

5. Results of iSOM-NIMBUS Procedure on Crash-worthiness Problem and Its Advantages

In this section, the proposed methodology to visualize the NIMBUS solutions using the iSOM approach is discussed in detail on the crash-worthiness problem (Vesikar et al., 2018). Crash-worthiness problem is an unconstrained MOO problem with three objective functions and five design variables. The decisions in various stages of the NIMBUS method adopted here are purely based on the author's choice. They allowed to demonstrate how the iSOM-aided NIMBUS procedure can be used conveniently. Any other decision by DMs can also be implemented similarly.

5.1. Using Complete Pareto-optimal Front

A scatter plot of a representative set of Pareto-optimal solutions in the entire search domain obtained using the NSGA-III procedure (Deb and Jain, 2014) is shown in the Fig. 2(a) in small dots as Step 1. In Step 2 the iSOM procedure is applied to the Pareto data set to obtain the component planes of each objective function. To facilitate our discussions, the objective vectors of the set are checked for clusters using the U-matrix in iSOM. U-matrix plot shows the existence of three different clusters in the entire Pareto set. The three clusters are seen and marked in the scatter plot in Step 3. Ideal, Utopian, and nadir points are estimated from the complete set for NIMBUS computations. The start point of the NIMBUS method is chosen to be around the centroid of the Pareto set and is marked with a black-colored diamond. This point falls in cluster 2. This completes Step 5. Lets say the DM chooses the start solution as: $\mathbf{x}^0 = (x_1, x_2, x_3, x_4, x_5) = (2, 2, 2, 2, 2)$ with start criterion vector $\mathbf{z}^0 = (f_1, f_2, f_3) = (1683.130, 9.630, 0.120)$, resulting in $\mathbf{z}^1 = (1668.870, 7.130, 0.090)$ on the Pareto-optimal front is shown in black face color in three iSOM component planes of the objectives. At the start point, a classification of objective functions is first defined by the DM, as follows:

$$I^< = \emptyset, I^{\leq} = \{2\}, I^{\geq} = \{1\}, I^= = \emptyset, I^{>} = \{3\},$$

with an aspiration level of $\bar{z}_2 = 6.85$ and $\varepsilon_1 = 1680$. This implies that DM wishes to improve on f_2 at the expense of increasing f_1 while letting f_3 change freely. Note that the above values need not be so specific and any other suitable values can also be chosen as desired by the DMs.

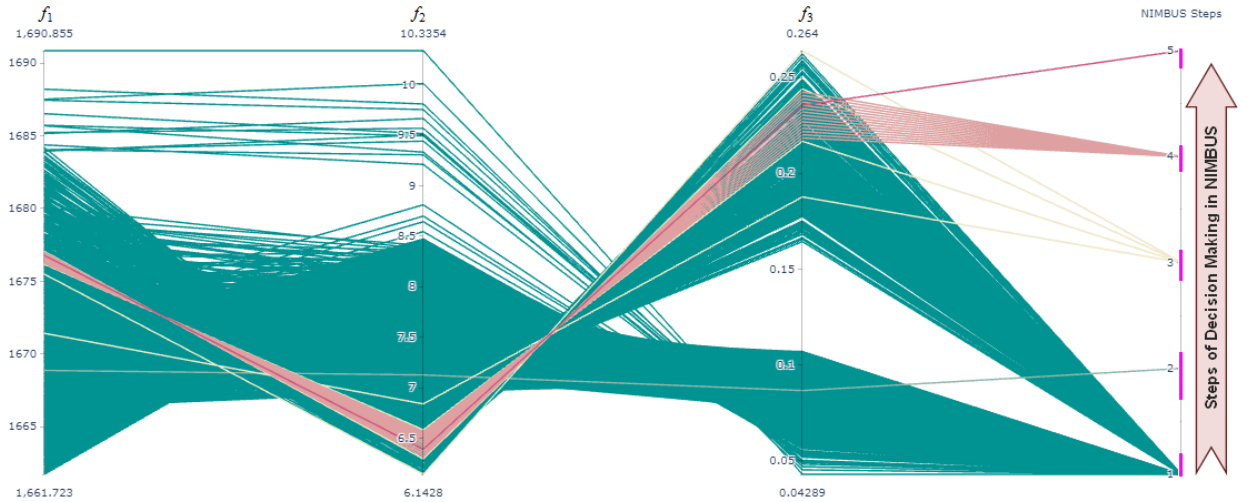


Figure 4: PCP on crash-worthiness problem: f_1, f_2 are f_3 are objective function axes, whereas NIMBUS Steps: 1 represents Pareto front, 2 represents start point, 3 represents alternate solutions, 4 represents intermediate solutions and 5 represents the final solution.

The un-selected cells after classification are shown by red edge color in the respective iSOM component planes of objectives. As objective f_3 can change freely, there are no un-selected points after classification. Hence, f_3 iSOM component plane has no cells with red edge color. The selected cells after classification are highlighted by white edge color in iSOM component plane of each objective. It is clear from the iSOM component planes that classification $I^{\leq} = \{2\}$ overrides $I^{\geq} = \{1\}$, as red edge color zone in f_2 iSOM component plane contains the red edge color zone in f_1 iSOM component planes. This completes Step 6. In Step 7, the resulting four MPB solutions are obtained based on the above classification. All the four MPB solutions with objective vectors $\mathbf{z}^{1,1} = (1671.421, 6.839, 0.188)$, $\mathbf{z}^{1,2} = (1675.490, 6.143, 0.264)$, $\mathbf{z}^{1,3} = (1676.166, 6.583, 0.217)$ and $\mathbf{z}^{1,4} = (1677.054, 6.295, 0.244)$ are different from the start-point \mathbf{z}^1 , so they are declared as alternate solutions. It is clear that two of the four alternate solutions (magenta face color) lie on the edge of the Pareto front. Also, the iSOM component planes of objectives indicate that the two alternate solutions in the edges have extreme values of f_2 and f_3 . In Step 5, if DM is not comfortable in choosing the edge points, DM is left with two intermediate alternate solutions $\mathbf{z}^{1,3}$ and $\mathbf{z}^{1,4}$, for which all three objectives seem to have a good compromise in them as Step 8. To create more points in the vicinity, the DM has an option of generating a maximum of $P = 15$ reference points in between them in Step 7. In Step 8, 15 different Pareto-optimal intermediate solutions are found solving AASF problem (Eqs.(2), (3), (4) and (5)) by classifying all objectives in $I^<$ class. Once

again, the iSOM component planes of objectives reveal that the intermediate solution (green face color) near the middle of all 15 intermediate solutions makes a better trade-off (near-average objective values of 15 intermediate solutions) in all three objectives. Thus, in Step 9, the intermediate solution marked using a red-faced cell is chosen. Since it is a Pareto-optimal solution, the NIMBUS method is terminated with the red-faced cell solution as the final solution $\mathbf{z}^2 = (1676.777, 6.392, 0.235)$ of the iSOM-NIMBUS procedure as Step 11.

5.2. Using a Focused Set of Pareto-optimal Solutions

It can be seen from Fig. 2 that most of the NIMBUS decision-making activities took place at the bottom-left corner of the iSOM component planes. DM's classification choice can take such activity anywhere on the Pareto-optimal front. A more clear visualization can be achieved if the decision-making activity can be carried out at a focused part of the Pareto-optimal front dictated by the alternate solutions obtained in Step 5. In this section, we take the help of a reference point-based NSGA-III procedure (Vesikar et al., 2018) for this purpose. We discuss the procedure here.

First, instead of NSGA-III, R-NSGA-III solutions are found and stored to create iSOM component planes. Reference point and shrinkage factor are calculated based on Equations (17) and (18) using the two chosen alternate solutions:

$$\begin{aligned}\mathbf{z}^r &= \frac{(1676.166, 6.583, 0.216) + (1677.054, 6.295, 0.244)}{2}, \\ &= (1676.610, 6.439, 0.230), \\ \mu &= \max \left[\frac{0.888}{33.492}, \frac{0.288}{4.603}, \frac{0.028}{0.225} \right], \\ &= \max [0.026, 0.063, 0.124], \\ &= 0.124.\end{aligned}$$

Next, iSOM component plane plots of objectives are made using R-NSGA-III solutions, and all 15 intermediate solutions including the two alternate solutions are marked in Fig. 3. For relevance, the R-NSGA-III solutions are also shown in the original scatter plot (Fig. 3(b)). It can be seen that 15 intermediate solutions are now more visible. The trade-off in objective values for 15 solutions is also clear, allowing the DM to make a choice in choosing the final solution (\mathbf{z}^2) with more confidence. The final choice is a solution that lies in the middle of the two alternate solutions for which all three objectives take an average value, making it a good trade-off solution among all 15 solutions. The color-contoured iSOM component plane plots of objective allow a DM to investigate the sensitivity of objectives in moving from one intermediate solution to the next and make a decision. This completes Step 10 of the iSOM-aided NIMBUS procedure.

5.3. Contrasting with NIMBUS Visualization Techniques

NIMBUS method includes several inbuilt visualization techniques. The parallel coordinate plot (PCP) (or the value path plot) is one of the best visualization techniques available in NIMBUS. In order to demonstrate the complete NIMBUS procedure on a PCP, we first show all NSGA-III-obtained Pareto-optimal solutions (Step 1 of NIMBUS procedure) in Fig. 4 with green lines for the crash-worthiness problem. We add a fourth vertical axis (in addition to three objective axes) to show the addition of NIMBUS points in different stages. The inclusion of NSGA-III solutions is the first stage of the PCP. In stage 2, the start-point (Step 2 of NIMBUS procedure) is shown with a white line. Four alternate solutions were found in Step 4 of NIMBUS procedure with yellow lines. The PCP clearly shows that all four solutions are associated with a small f_2 value and a relatively high f_3 value. By looking at the PCP, it is difficult to conclude that two of the four alternate solutions lie on the edge of the Pareto-optimal front. Only one of the four solutions has the largest f_3 value and smallest f_2 value. While this solution can be considered to lie on the edge, the second near-edge solution is difficult to comprehend. In comparison, iSOM component plane of objectives in Fig. 2 clearly shows that two alternate solutions lie close to the edge of the Pareto front.

Next, in stage 4, 15 intermediate solutions are shown with red lines. While they lie in between the two pivoting alternate solutions chosen to create them, some trade-off in objectives can be observed from the PCP. But the true trade-off among the solutions is not apparent. The final solution chosen using iSOM-NIMBUS procedure is marked in stage 5, but if an average trade-off solution would have been the choice, a different solution passing through the middle of two pivoting alternate solutions in each objective axes should have been chosen. Clearly, the PCP does not provide a true idea of the location of a point in the perspective of the entire Pareto-optimal front. PCP does not also provide true trade-off information. It certainly cannot show clusters, holes, and discontinuity in the Pareto-optimal

Table 2

NIMBUS-iSOM solutions on benchmark and real-world problems discussed in the main paper. NIMBUS solutions, shown in bold indicate two pivotal solutions to create intermediate solutions. $N_{\bar{z}}$ indicates the number of intermediate solutions generated. The ideal point (z^*), final solution (\hat{z}), and nadir point (z^{nad}) are shown in the final column in that order.

Problem	Start Point (z_1)	Classification	Alternate Solutions (\hat{z})	$N_{\bar{z}}$	z^*, \bar{z}, z^{nad}
Crash-worthiness	(1668.868, 7.126, 0.087)	$f_1 \geq 1668.868$, $f_2 \leq 7.126$, $f_3 < 0.087$.	(1671.421, 6.839, 0.188); (1675.490, 6.143, 0.264); (1676.166, 6.583, 0.217) ; (1677.054, 6.295, 0.244) .	15	(1661.708, 6.143, 0.039); (1676.777, 6.392, 0.235); (1695.200, 10.745, 0.264).
Naru-weiss	(-5.509, -2.946, -7.177, 0.436, 0.016)	$f_1 < -5.509$, $f_2 < -2.946$, $f_3 \geq -7.177$, $f_4 \geq 0.436$, $f_5 < 0.016$.	(-6.340, -3.426, -0.321, 8.694, 0.350); (-6.283, -3.252, -3.129, 3.485, 0.325); (-6.307, -3.257, -2.208, 3.549, 0.336) ; (-6.222, -2.967, -4.500, 0.450, 0.298) .	15	(-6.340, -3.445, -7.500, 0.000, 0.000); (-6.275, -3.091, -3.348, 1.387, 0.322); (-4.751, -2.867, -0.321, 9.706, 0.350).
DTLZ-7	(0.155, 0.155, 5.380)	$f_1 \geq 0.155$, $f_2 \geq 0.155$, $f_3 \leq 5.380$.	(0.251, 0.251, 5.147); (0.855, 0.855, 2.616); (0.717, 0.717, 3.902) ; (0.668, 0.668, 4.645) .	15	(0.000, 0.000, 2.615); (0.683, 0.683, 4.415); (0.859, 0.859, 5.955).
C2DTLZ2	(0.577, 0.577, 0.577)	$f_1 \leq 0.577$, $f_2 < 0.577$, $f_3 \leq 0.577$.	(0.000, 1.000, 0.000); (0.067, 0.920, 0.386) ; (0.186, 0.920, 0.345) .	15, 15	(0.000, 0.000, 0.000); (0.035, 0.979, 0.197); (1.000, 1.000, 1.000).
Carside Impact	(31.179, 3.756, 11.411)	$f_1 > 31.179$, $f_2 \leq 3.756$, $f_3 < 11.411$.	(37.869, 3.585, 11.066); (32.731, 3.669, 11.578) ; (34.305, 3.591, 11.748) .	15	(23.748, 3.585, 10.611); (33.293, 3.639, 11.640); (41.199, 3.987, 12.491).
WATER	(0.830, 0.266, 0.325, 0.419, 0.861)	$f_1 < 0.830$, $f_2 < 0.266$, $f_3 < 0.325$, $f_4 < 0.415$, $f_5 < 0.861$.	(0.819, 0.500, 0.250, 0.573, 0.565); (0.817, 0.633, 0.227, 0.632, 0.479) ; (0.818, 0.566, 0.237, 0.604, 0.519) .	15	(0.798, 0.027, 0.095, 0.031, 0.001); (0.817, 0.599, 0.232, 0.618, 0.498); (0.918, 0.900, 0.950, 1.350, 3.140).
GAA	(73.87, 1885.35, 59.33, 1.97, 450.33, 42665.30, -2145.27, -15.33, -197.96, 1.08)	$f_1 < 73.87$, $f_2 < 1885.35$, $f_3 < 59.33$, $f_4 < 1.97$, $f_5 < 450.33$, $f_6 < 42665.30$, $f_7 < -2145.27$, $f_8 < -15.33$, $f_9 < -197.96$, $f_{10} \geq 2.00$.	(74.745, 2039.188, 85.483, 2.538, 360.318, 45270.785, -2041.393, -19.259, -192.681, 2.895); (73.246, 2115.349, 87.119, 2.388, 331.409, 46531.275, -2354.166, -19.296, -187.258, 2.042); (73.276, 1957.045, 77.198, 2.646, 483.566, 43470.697, -2997.576, -16.516, -192.592, 1.604) .	15	(73.18, 1826.54, 54.22, 1.76, 231.32, 41324.27, -3121.66, -20.64, -209.69, 0.00); (73.28, 1950.27, 75.00, 2.26, 447.82, 43172.46, -2756.46, -16.17, -189.35, 2.05); (75.23, 2154.92, 97.31, 2.61, 552.19, 47912.62, -883.57, -13.98, -182.58, 4.68).

front. Hence, reliable visualization-based decision-making becomes a difficult task using PCP. They can be used to passively demonstrate a set of trade-off solutions, as a trade-off in objectives occurs only if there is criss-crossing of lines in two neighboring objective axes in a PCP.

5.4. Involving Human Decision-makers

In order to obtain a direct feedback from real decision-makers, we have involved four DMs (two professors from Indian Institute of Technology, Guwahati and Madras in India, and two doctoral students from the latter) having expertise and knowledge in design and optimization topics. They have been provided with a brief tutorial on the working principles of NIMBUS and iSOM procedures. Then, they were asked to apply a few iterations of the iSOM-NIMBUS procedure to the crash-worthiness and a few other test problems. The details of their feedback on the advantages of using the integrated iSOM-NIMBUS procedure are outlined in the supplementary document, but in general, they all have positively commented on the role of the visual aid provided by the iSOM approach in executing the NIMBUS procedure.

6. Results on Benchmark Problems

6.1. The five-objective Problem from NIMBUS Study

Naru-weiss problem is a two-variable, five-objective unconstrained multi-objective optimization problem (Miettinen and Mäkelä, 2000). The formulation for this problem is given in the supplementary document. In Fig. 5(a), three

objectives f_1 , f_2 and f_3 are represented on three axes. f_4 is represented by the marker size (proportional to its value) and f_5 is represented by the color (blue to yellow indicating low to high value).

From Fig. 5(a), it is clear that the objective functions f_1 and f_3 are conflicting in nature. Also, f_2 and f_4 are in conflict to each other. The objective function f_5 has a small value at one certain location (dark blue region) and then increases rapidly outwards from that location. The same inference can be drawn from the component plane of objective functions depicted in Fig. 5(b).

From the start point (dark black cell indicating minimum of f_5), DM provides the following classification of objectives:

$$I^< = \{1, 2\}, I^{\leq} = \emptyset, I^{\geq} = \{3, 4\}, I^= = \emptyset, I^{>} = \{5\},$$

with $(\epsilon_3, \epsilon_4) = (-4.5, 0.45)$ (worsening f_3 and f_4 till some limit), letting f_5 change freely and hoping to improve f_1 and f_2 as much as possible.

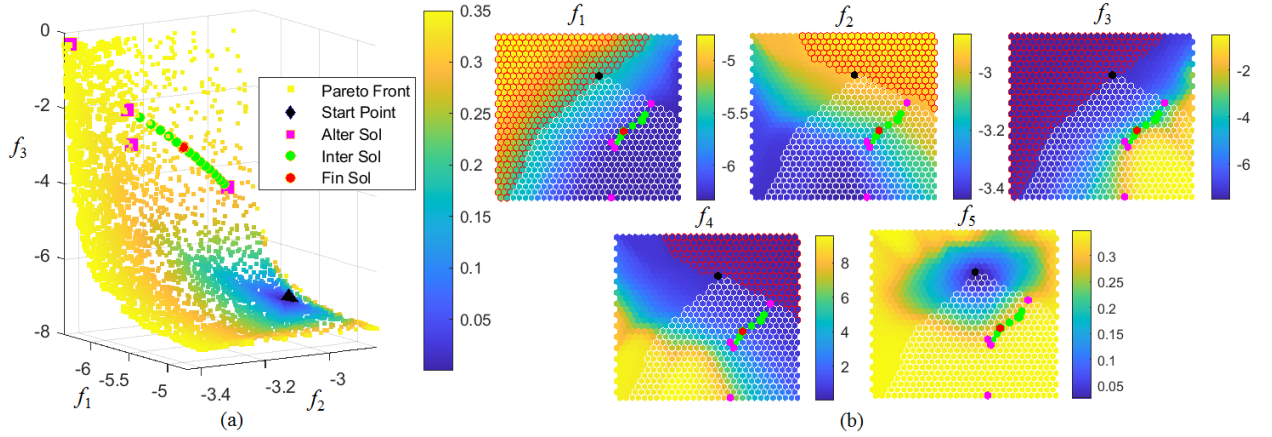


Figure 5: Naru-weiss problem (a) 5-d Scatter plot obtained from NSGA-III Pareto optimal points, f_1, f_2 and f_3 on axes, f_4 is represented by marker size and f_5 is represented by the color bar, Selected part of search space after classifications are shown by blue markers, (b) iSOM component planes of objective functions f_1, f_2, f_3, f_4 and f_5 . Un-selected points and selected points in search space after classification and all the NIMBUS critical points have been represented by cells with the color code scheme provided in Table 1.

Four sub-problem formulations find four independent alternate solutions, marked with magenta cells. One alternate solution at the edge of the Pareto front is discarded. Then, randomly two out of three alternate solutions are selected and 15 intermediate solutions are computed in between them using the procedure described in Step 9 of the iSOM-aided NIMBUS procedure, of which one solution (red face cell) is chosen as the final solution (see Table 2 for a summary of iterative solutions for this and other problems of this paper). The start point, alternative and intermediate solutions, and the final solution are marked in Fig. 5, using the color code defined in Table 1.

If we observe the iSOM component planes of objectives, we can conclude that the start point corresponds to small values of f_3 , f_4 , and f_5 , whereas moderate values of f_1 and higher values of f_2 can also be verified from the scatter plot in Fig. 5(a) as well. Out of two alternate solutions, one alternate solution corresponds to a large value of f_2 , f_3 and f_5 component planes, whereas small values of f_1 and f_4 planes that can be verified from scatter plot in Fig. 5(a) as well. It is evident from Fig. 5(b) that the intermediate solutions spread in large values of f_5 component plane, but have small values of f_1 and f_4 component planes and span across large to small values in f_2 and f_3 component planes. The final solution (shown as a red face cell) makes a good compromise in values of all five objectives among 15 intermediate solutions. Besides making a good compromise, the final solution is also away from the Pareto boundary and well inside the feasible space. Without the iSOM component plane plots of the objectives, such decision-making would have been difficult to achieve. The final solution is sent to Item 10 of NIMBUS algorithm for a final Pareto-optimality check before termination of the overall NIMBUS-iSOM procedure. The iSOM component planes of objectives also allow DM to have clear ideas of (i) centrality (or boundary) of the solutions in the Pareto-optimal front, (ii) proximity to constraint boundaries, and (iii) a trade-off among objectives. The methodologies described in the PaletteViz study (Talukder and Deb, 2020; Deb and Talukder, 2021) in identifying *knee* point, a hole, and other peculiarities can be considered and marked appropriately on the iSOM component planes for additional aid in decision-making.

6.2. A Disjoint Pareto Set Problem: DTLZ7

DTLZ7 problem has three objective functions and the Pareto optimal front is separated by four disjoint regions (Li et al., 2016). The scatter plot of the Pareto-optimal front obtained using NSGA-III and their classification, obtained using the U-matrix of the iSOM component planes, into four clusters are shown in Fig. 6(a). The start point is shown with a blue diamond, which happens to fall on cluster 3. The following classification is made by the DM:

$$I^< = \emptyset, I^{\leq} = \{3\}, I^{\geq} = \{1, 2\}, I^= = \emptyset, I^{>} = \emptyset,$$

with $\bar{z}_3 = 5.25$ (improving f_3 with a limit) and $(\epsilon_1, \epsilon_2) = (0.859, 0.859)$ values (at the expense of worsening f_1 and f_2 within limits).

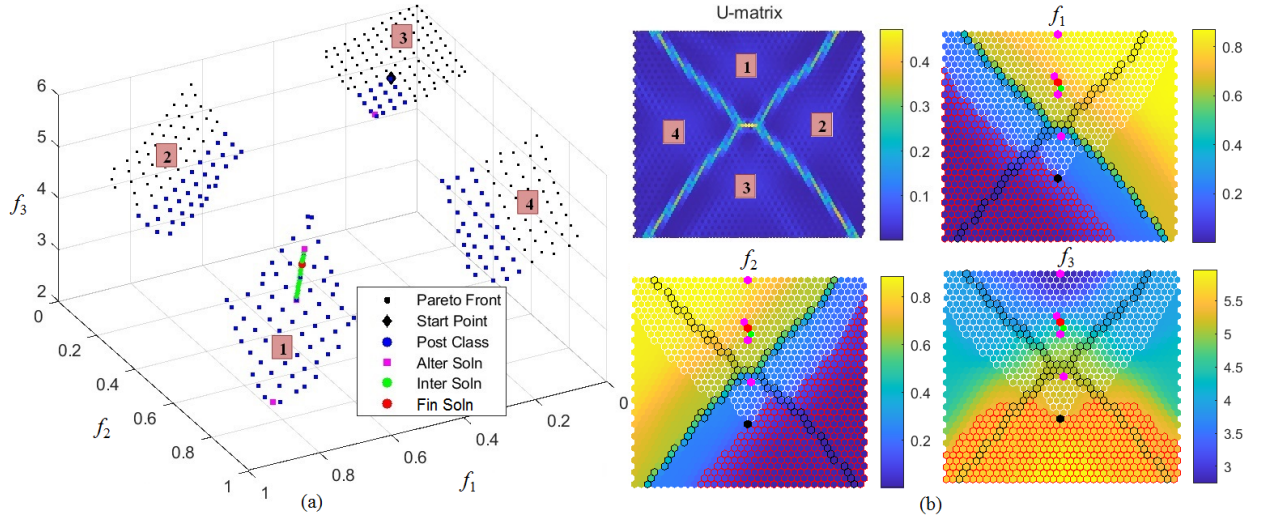


Figure 6: DTLZ7 problem: (a) NSGA-III-obtained Pareto points and the NIMBUS solutions. Selected part of search space after classification is shown by blue markers. (b) iSOM component planes of objectives, selected and un-selected points after classification and all critical NIMBUS points.

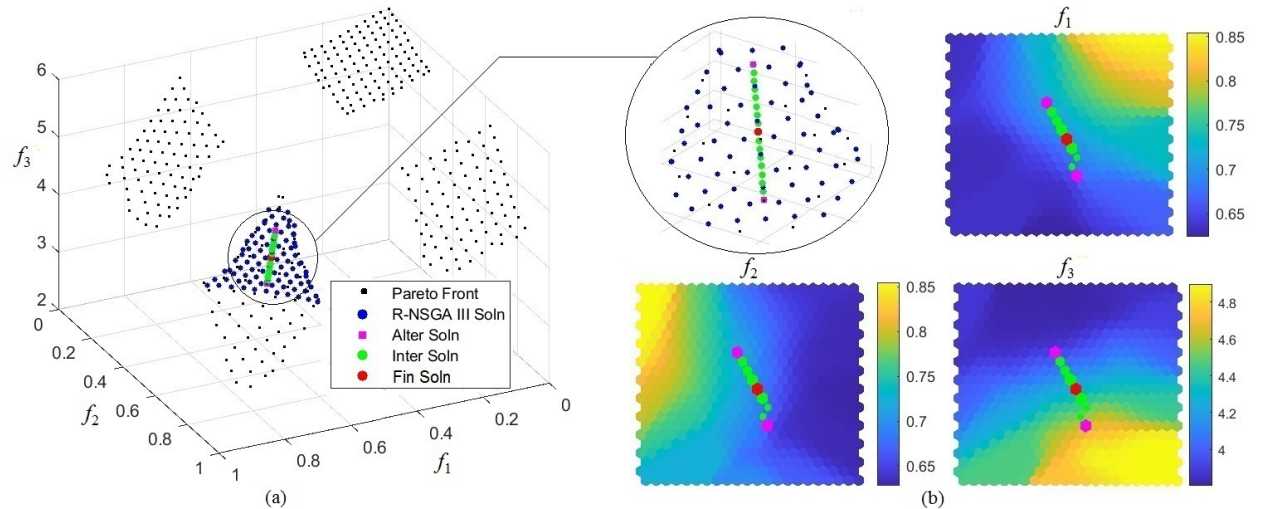


Figure 7: DTLZ7 problem: (a) R-NSGA-III-obtained Pareto points and the NIMBUS solutions. (b) iSOM component planes of objectives using focused Pareto points and all critical NIMBUS points.

The selected points after classification are shown with blue marker color in the Fig. 6(a). The respective iSOM component planes of objectives are shown in Fig. 6(b). It is clear that the start point falls on cluster 3 and is somewhat

away from the Pareto boundary. Step 7 finds four alternate solutions, marked with magenta face color. These points are marked on the iSOM component planes of objectives. Clearly, despite the start point's location in cluster 3, the alternate solutions obtained by solving four sub-problems produce three points on cluster 1 and one in cluster 3. These points are also marked in the scatter plot in Fig. 6(a) for clarity, but a good idea of the location of all four alternate points is clear from iSOM component plane plots of the objectives. At Step 8, two preferred alternate solutions – two interior points having a good trade-off among all three objectives – are chosen by the DM. In Step 9, 15 intermediate solutions (marked in green cells) are found systematically within the two preferred alternate solutions. Finally, a solution from the center region of all intermediate solutions is chosen as the final solution (shown with a red cell). A final Pareto-optimality check of the final solution will terminate the decision-making process.

In this problem, the two chosen alternate solutions and the resulting 15 intermediate solutions lie in one of the four clusters (cluster 1). To have a more clear visualization and decision-making, R-NSGA-III can be employed to obtain a set of focused Pareto-optimal points to develop iSOM component plane plots of the objectives using the reference point $\mathbf{z}^r = (0.7863, 0.7863, 3.2591)$ and shrinkage factor $\mu = 0.2$. Fig. 7(a) re-plots the scatter plot with R-NSGA-III points. Fig. 7(b) shows iSOM component planes of objectives using R-NSGA-III points only. The two preferred alternate solutions and 15 intermediate points are also marked on the iSOM component planes of objectives. The final solution can now be seen to lie at a good compromise region of each objective and almost at the center of the R-NSGA-III obtained Pareto-optimal region. Whenever more focused decision-making needs to be performed to better visualize the trade-off in objectives, the original NSGA-III can be replaced with R-NSGA-III to find a focused set of points for clarity and more convenient decision-making.

6.3. Constrained Problem: C2-DTLZ2

Next, we consider a constrained test problem: three-objective C2-DTLZ2 problems. NSGA-III points are shown in Fig. 8(a). Decision-making in the presence of constraints requires a clear visualization framework revealing near-constraint solutions. This problem is chosen to demonstrate the effectiveness of iSOM visualization method for this purpose.

The iSOM U-matrix plot reveals that there are four clusters in the Pareto-optimal front and also identifies the boundary points of each cluster. The boundary points, marked with grey markers, happen to fall on the constraint boundary. The start point is found to be at the center of the complete Pareto-optimal front, marked with a black diamond. The iSOM component planes shown in Fig. 8(b) also mark the start point. The boundary of each cluster is also clearly shown in iSOM component plane plots of the objectives. The following classification rules are provided for this problem:

$$I^< = \emptyset, I^{\leq} = \{1, 3\}, I^{\geq} = \emptyset, I^= = \emptyset, I^{>} = \{2\},$$

with $(\bar{z}_1, \bar{z}_3) = (0.3, 0.5)$ (improve f_1 and f_3 to their limits) at the expense of possible worsening of f_2 without any limit.

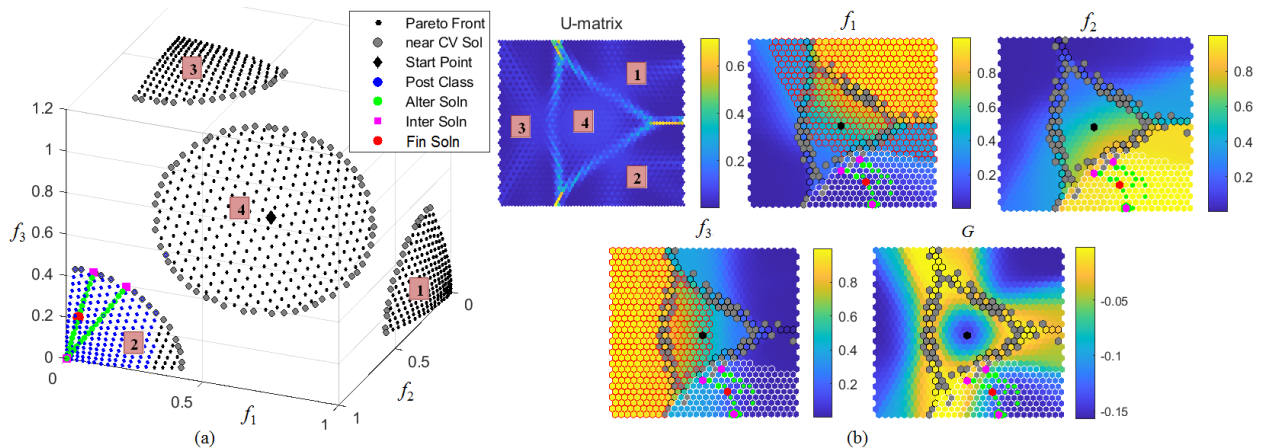


Figure 8: C2DTLZ2 problem: (a) NSGA-III-obtained Pareto points, NIMBUS solutions and selected part of search space after classification. (b) iSOM component planes of objectives using complete Pareto points, selected and un-selected points after classification and all critical NIMBUS points.

Notice that four sub-problems in Item 3 of NIMBUS algorithm produce three alternate solutions, marked with magenta cells in iSOM component plane plots of the objectives. Of these three points, two fall on the constraint boundary and one at the extreme of cluster 2. The nearness of constraint boundary and extreme position on cluster 2 is clear from iSOM component planes as well. Each of the constraint boundary solutions is paired up with the extreme solutions and 15 intermediate solutions are found for each pair. It can be seen from iSOM component plane plots of the objectives that all 30 intermediate solutions correspond to small values of f_1 , large values of f_2 , and small to intermediate values of f_3 . A good compromise solution lying close to the centroid of the intermediate solutions is chosen as the final solution (shown in red color).

A separate iSOM component plane plot for the constraint is shown for this problem. The near constraint cells, boundary points, and ensuing alternate and intermediate solutions are shown in the plot, allowing DM to choose a final solution that is away from the constraint boundary but also not too close to the extreme Pareto solution. This level of visualization and understanding of Pareto-optimal points on the entire Pareto front or a focused part of the Pareto front is rare in standard Pareto visualization methods. Despite requiring several iSOM component planes, they, together, allow a more convenient decision-making environment revealing critical functionalities associated with a problem. This example demonstrates the sensitivity of the decision-making task in arriving at a final preferred solution and the importance of an easier and more revealing visualization framework for performing convenient and effective decision-making for multi- and many-objective optimization.

7. Results on Real-world Problems

7.1. Carside impact problem

Carside impact problem is a three-objective, 10-constraint problem, in which the weight of the car, the pubic force experienced by a passenger, and the average velocity of the B-pillar responsible for withstanding the impact load need to be minimized (Deb and Kumar, 2007a). This problem will allow us to demonstrate the iSOM-based visualization in the presence of constraint/s on a real-world problem.

NSGA-III points are shown in Fig. 9(a) for a reference since the objective space is three-dimensional. The resulting iSOM component planes (three objectives and constraint violation) are shown in Fig. 9(b). Note that a non-zero constraint violation $G(\mathbf{x})$ point (Eqn. (16)) implies it is feasible. The start point on the Pareto front is shown with a black colored cell on all four iSOM component planes. At the start point ($\mathbf{z}^1 = (31.180, 3.756, 11.411)$), the DM makes the following classification:

$$I^< = \emptyset, I^{\leq} = \{2\}, I^{\geq} = \emptyset, I^= = \emptyset, I^{>} = \{1, 3\}.$$

This means the DM wishes to improve f_2 with a limit $\bar{z}_2 = 3.75$ and allow f_1 and f_3 to change freely.

Fig. 9 (both a and b) shows the possible cells (or solutions) that satisfy the above classification and are selected for further search. The respective cells are marked with white-bordered cells and the un-selected cells are marked with red-bordered cells. Cells that are close to the constraint boundary are marked in grey color. Step 7 produces three distinct alternate solutions, marked in magenta color. Two alternate solutions are far away from the constraint boundary and also are at the boundary of the Pareto front, as can be confirmed from the scatter plot shown in Fig. 9(a). Choosing the two solutions on the selected part, 15 intermediate solutions (shown in green) are created in Step 9. Among these 15 solutions, the final solution, marked in red color, makes a good compromise in keeping f_1 and f_3 objectives not too worse, while forcing f_2 to go close to $\bar{z}_2 = 3.75$. The final solution is $\bar{\mathbf{x}} = (0.50, 1.35, 1.29, 1.50, 2.11, 1.20, 0.40)$ with $\bar{\mathbf{z}} = (33.293, 3.639, 11.640)$. It can be seen that this final solution is better than \mathbf{z}^1 in f_2 (reduced from 3.756 to 3.639) with slightly worse values in both f_1 (increased from 31.180 to 33.293) and f_3 (increased from 11.411 to 11.640). Although the desired target of $\bar{z}_2 = 3.75$ too close to $z_2^1 = 3.756$ was supplied in the classification step, the final solution has a smaller value than $\bar{z}_2 = 3.75$, which is allowed.

7.2. WATER Problem

WATER problem has five objectives and seven constraints (Deb et al., 2002). As discussed earlier, in order to visualize the near constraint violation Pareto optimal solutions, we compute the average of the normalized constraint violation and plot a separate component plane G using iSOM. Fig. 10(a) represents the scatter plot of the NSGA-III obtained Pareto front. Objectives f_1 , f_2 , and f_3 are represented on axes, f_4 is represented by marker size, and f_5 is represented on a color scale. Larger marker size and yellow marker color indicate the larger value of f_4 and f_5 , respectively. This scatter plot is used only for verification purposes here. The NIMBUS solutions – start point, alternate

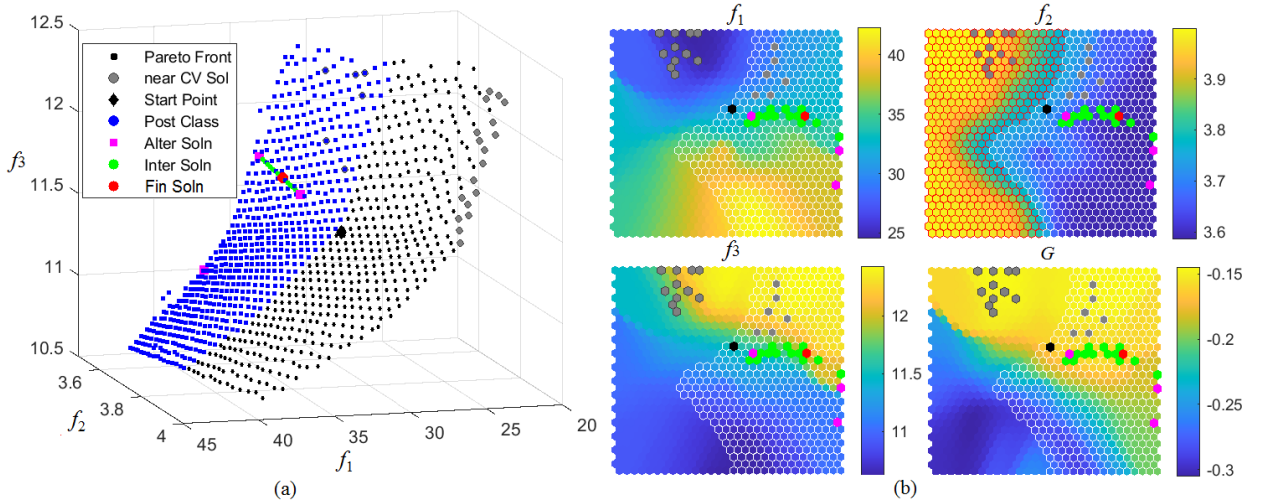


Figure 9: Carside impact problem: (a) NSGA-III-obtained Pareto points and the NIMBUS solutions. Selected part of search space after classification. (b) iSOM component plane plots of the objectives using complete Pareto points, selected and un-selected points after classification and all critical NIMBUS points.

solutions, intermediate solutions, selected and un-selected points after classification, near-constraint solutions, and the final solution are plotted on the scatter as well as the iSOM component planes. The start point is shown with a black cell. Clearly, iSOM component planes of objectives indicate that f_1 and f_3 are highly correlated, while others have trade-offs. Also, the start point is far away from the constraint boundary. The classification provided by the DM is shown below:

$$I^< = \{1, 3, 5\}, I^{\leq} = \emptyset, I^> = \emptyset, I^= = \emptyset, I^{<>} = \{2, 4\}.$$

DM wishes to improve f_1 , f_3 , and f_5 without any limit at the expense of possible worsening of f_2 and f_4 without any limit. Selected and un-selected cells are shown on iSOM component planes.

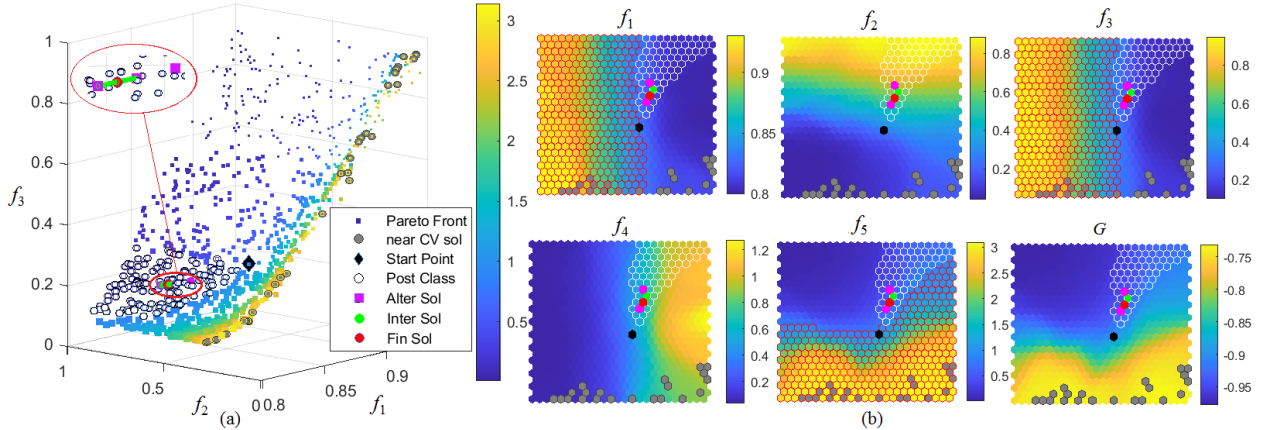


Figure 10: WATER problem: (a) NSGA-III-obtained Pareto points, NIMBUS solutions and selected part of search space after classification. (b) iSOM component planes of objectives using complete Pareto points, selected and un-selected points after classification and all critical NIMBUS points. In iSOM component plane one alternate solution and the final solution have shared the same node.

Three alternate solutions, marked with magenta color, are found by the NIMBUS procedure. The iSOM component planes make it clear that all three solutions lie on the selected part of the Pareto front and are far away from the constraint boundary. Also, it is clear that the alternate solutions do not unnecessarily make $I^{<>}$ -class objectives too worse (not

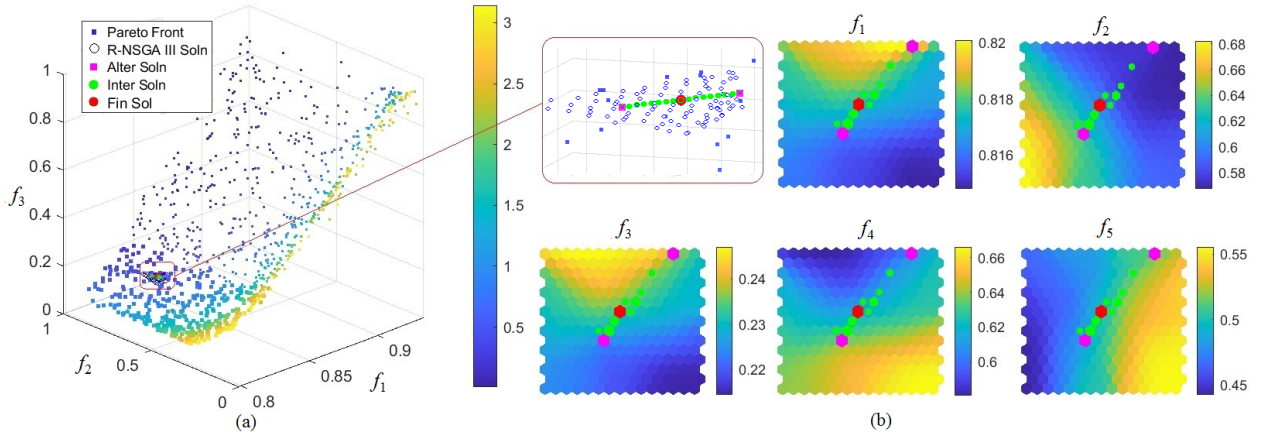


Figure 11: WATER problem: (a) R-NSGA-III-obtained Pareto points and the NIMBUS solutions. (b) iSOM component planes of objectives using focused Pareto points and all critical NIMBUS points. The R-NSGA-III-obtained Pareto points in hollow blue markers are blown up for clarity.

taking them to yellow cells) while improving $I^<$ -class objectives slightly from the start point. The trade-offs in the objectives do not allow these alternate points to be away from each other.

To investigate the alternate solutions better, we apply R-NSGA-III using reference point (0.817, 0.600, 0.232, 0.618, 0.499) and shrinkage factor of 0.1 to obtain more focused Pareto points. They are used to create a new set of iSOM-plots, which is presented in Fig. 11. Since the third alternate solution is relatively closer to the start point than the other two alternate solutions, hence for the given classification the third solution is worse than the other two alternate solutions. Therefore, the other two alternate solutions that are away from the start point are selected. 15 intermediate solutions are found using two chosen alternate solutions and are shown in green color. Eventually, the final solution, marked in red color, is found by observing a good compromise of intermediate solutions.

The final solution is $\tilde{\mathbf{x}} = (0.303, 0.024, 0.010)$ having $\tilde{\mathbf{z}} = (0.817, 0.600, 0.232, 0.618, 0.498)$. From the start point (\mathbf{z}^1) (see Table 2), the final solution is better in f_1 , f_3 and f_5 with a deterioration in f_2 and f_4 , as desired by the classification. The use of iSOM-based visualization has helped in the process of arriving at the final solution by allowing the DM to have a comprehensive look at the entire Pareto set from its proximity to constraint boundary and objective trade-offs.

7.3. 10-objective GAA Problem

General Aviation Aircraft (GAA) is a 10-objective problem (Simpson et al., 1996) consisting of 27 decision variables and 18 constraints. A set of well-converged Pareto-optimal solutions is generated using NSGA-II to plot the iSOM component plane of objective functions (f_i ; $i = 1, \dots, 10$), an average of normalized constraint violation (G), as shown in Fig. 12. For this problem, we introduce a new but important decision-making metric – trade-off (T) of the objectives in the neighborhood of a solution. It is the ratio of the average loss to average gain in objective values in favor of neighboring solutions (Deb and Talukder, 2021). A solution having higher T means that loss per unit gain is more for choosing a neighboring solution instead of the current solution; hence, it is wise to stay with the current solution as a preferred option. From the iSOM component planes, the conflicting behavior among the objective functions can be observed. The near-zero CV solutions are shown by grey-colored iSOM cells in objective functions and G component plane. After visualizing the near-zero CV solutions, DM may wish to select a start point that is far from the region (grey-colored iSOM cells) having relatively larger CV values (infeasible solutions). At the start point $\mathbf{z}^1 = (73.87, 1885.35, 59.33, 1.97, 450.33, 42665.30, -2145.27, -15.33, -197.96, 1.08)$ (shown in black color cell in Fig. 12), the classification defined by the DM is

$$I^< = \{1\}, \quad I^{\leq} = \emptyset, \quad I^{\geq} = \{10\},$$

$$I^= = \emptyset, \quad I^{>} = \{2, 3, 4, 5, 6, 7, 8, 9\},$$

with $\epsilon_{10} = 2.0$ to improve the objective function f_1 at the cost of increasing f_{10} , while letting freely change other eight objective functions.

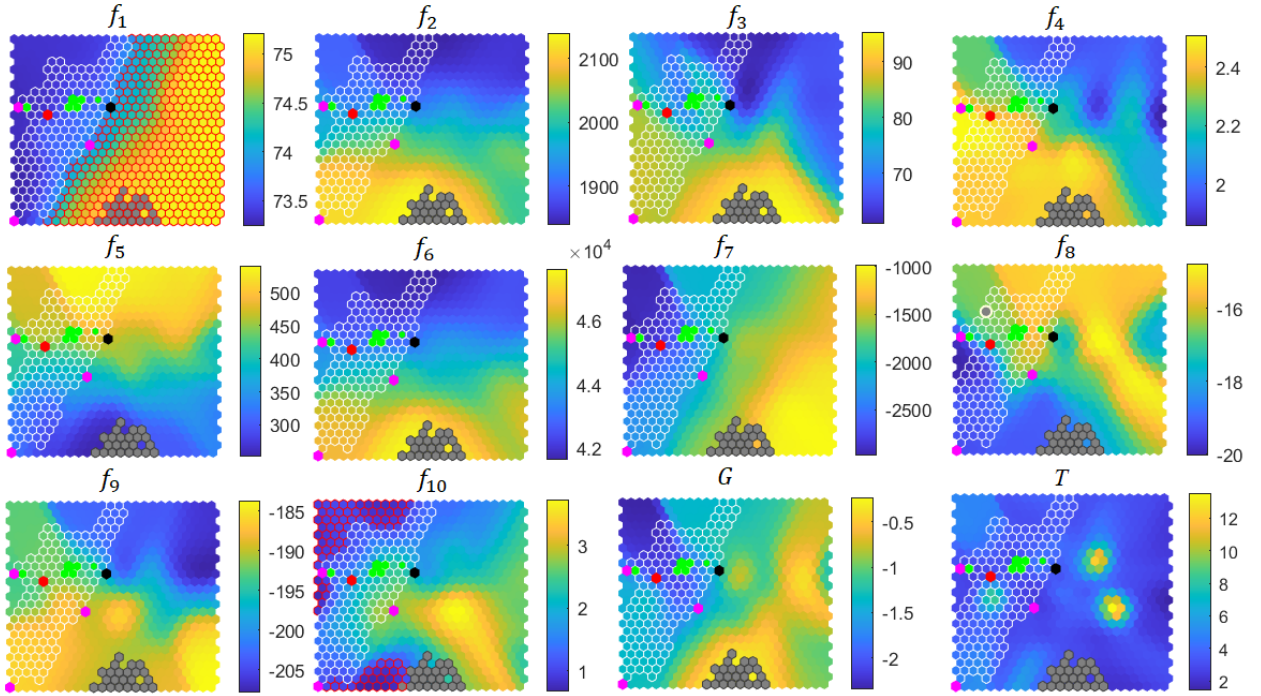


Figure 12: GAA problem: iSOM component planes of objectives using complete Pareto points, selected and un-selected points after classification, and all critical NIMBUS points- start point, alternate solutions, intermediate solutions, and final solution.

Selected and un-selected regions are highlighted in iSOM component planes as per the color code defined in Table 1. Upon solving the scalarized sub-problems, three different alternate solutions $\mathbf{z}^{1,1}$, $\mathbf{z}^{1,2}$, $\mathbf{z}^{1,3}$ are obtained and plotted on iSOM component planes with magenta color cells. It is observed that all three alternate solutions lie at boundary of the selected region obtained after the classification step. Also, two of the three alternate solutions ($\mathbf{z}^{1,1}$ and $\mathbf{z}^{1,2}$) lie at higher values of f_2 , f_3 , f_4 , f_6 and f_9 . Say, the DM decides to select an alternate solution ($\mathbf{z}^{1,3}$) that lies at higher values of f_4 and f_5 , whereas moderate values of f_9 , and at relatively low values of other objectives. Next, 15 intermediate solutions are generated between the start point \mathbf{z}^1 and the selected alternate solution $\mathbf{z}^{1,3}$ and are shown in green colored iSOM cells. Since DM wished to improve f_1 while allowing to deteriorate f_{10} , iSOM plots reveal that intermediate solutions that have lower f_1 values are (i) at the edge of the selected region (white color cell boundaries), (ii) come with higher values of f_3 and f_4 , and (iii) has relatively lower trade-off values. Thus, the DM needs to look at iSOM plots for an intermediate solution that (i) is far from the edge of the selected region, (ii) has moderate f_3 and f_4 values, and (iii) has relatively high trade-off values. The T -iSOM plot shows the marked red point (one of the intermediate points) has the largest relative trade-off value and better objective values of all objectives, except f_4 . These visual comparisons of intermediate points lead to the final solution: $\bar{\mathbf{z}} = (73.29, 1950.27, 75.00, 2.26, 447.82, 43172.46, -2756.46, -16.17, -189.35, 2.05)$. We observe that this final solution ($\bar{\mathbf{z}}$) has an improved f_1 value from 73.87 to 73.28 with a deterioration of f_{10} from 1.08 to 2.05 compared to \mathbf{z}^1 . This example shows how the iSOM visualization can aid the decision-maker to investigate alternate trade-off solutions, focus on a few, and then choose a preferred one being guided by NIMBUS's decision-making steps involving classification and prescribed limits on objective values.

Although our proposed iSOM visualization method requires DMs to consider a linearly increasing number of iSOM plots with number of objectives, this 10-objective example and our decision analysis reveal an important matter. In addition to objective iSOM plots, functionally important iSOM plots, such the trade-off (T) iSOM plot to help choose a solution that would cause a large loss per unit gain in case a neighboring solution was preferred, constraint violation (G) based iSOM plot to help choose a solution away from constraint boundaries, other problem-specific utility function based iSOM plots (Kennedy et al., 2008), or robust and reliability based iSOM plots preferring solutions with certain desired properties, can provide more relevant and direct decision-making information to the DMs. Moreover, a few functionally motivated iSOM plots can be a way to scale-up the visualization aspect of the decision-making procedure

for many-objective problems. Objective iSOM plots can stay as secondary visual decision-making aid, but primary selection of non-dominated points can be obtained using functionally motivated iSOM component planes.

8. Conclusions

In multi-criterion decision-making (MCDM), an effective visualization of Pareto-optimal solutions to have clear visual information about the extent of constraint closeness/violation, distance from the edge of Pareto-optimal front, trade-offs among the objectives, robustness and other point measures should provide vital information to the decision-maker (DM) in arriving at a preferred solution(s) in each iteration of the respective MCDM procedure. The usual visualization methods used in MCDM activities, such as parallel coordinate plots, radial visualization, scatter plots, etc. are various geometric techniques to present higher-dimensional Pareto-optimal solutions in a two-dimensional plot, but cannot provide any *functional* information that can help a DM. In this paper, we have proposed an interpretable self-organizing map (iSOM) approach which makes two-dimensional maps of each objective and constraint violation functions from Pareto solutions to provide a comprehensive picture of solutions, their trade-offs, nearness to constraint boundaries, etc. We have briefly discussed the iSOM approach and indicated how the original NIMBUS decision-making procedure can be aided with iSOM component planes in aiding a DM task. We have proposed a color and style scheme for visualizing each cell of iSOM to clearly show (i) cells with function-value-based coloring, (ii) near-constraint cells, (iii) the starting cell for NIMBUS procedure, (iv) cells that satisfy (and do not satisfy) NIMBUS classification of objectives, (v) alternate NIMBUS-obtained solutions meeting classification conditions, (vi) created intermediate solutions from a chosen set of alternate solutions, and (vii) the final preferred solution. iSOM component planes can help DMs to make decisions in most of their steps by visualizing two-dimensional iSOM component planes. For clarity, the procedure has been aided with creating iSOM component planes with focused Pareto points obtained using R-NSGA-III procedure at the preferred part of the Pareto front.

The iSOM-NIMBUS procedure has been demonstrated on a number of constrained and unconstrained numerical problems and real-world problems from three to ten-objective problems. The detailed description of the plots has helped to understand the NIMBUS procedure better and importantly has demonstrated how iSOM visualization with points, either from the complete Pareto set or from a part of the Pareto set, has proposed an informed decision-making aid to the use of the NIMBUS procedure. Based on the visualization aspects of an interactive MCDM, an assessment of iSOM has been performed on different steps of NIMBUS by involving human DMs, who commented positively on the convenience and benefits of using the iSOM visualization technique with the MCDM approach.

The iSOM visualization methodology is now ready to be used with other MCDM procedures, such as Pareto race (Korhonen and Wallenius, 1988; Korhonen and Yu, 2000), STOM (Nakayama and Sawaragi, 1984), GUESS (Buchanan, 1997) and other methods (Miettinen, 2012). A layered iSOM approach in which higher-level iSOM cells can be expanded with lower-level iSOM cells in a hierarchical manner can be implemented to focus on larger to smaller areas on the Pareto-optimal front. Focused EMO procedures, such as R-NSGA-III (Vesikar et al., 2018), can be run quickly using a parallel computing environment to enable such transitions smoothly. Other key features of Pareto-optimal solutions, such as knee points having large trade-off among objectives, holes, robust/reliable solutions against uncertainties, etc. can also be implemented in the iSOM approach for easy visualization (Talukder and Deb, 2020; Deb and Talukder, 2021). Nevertheless, this paper has shown the importance of bringing multi-criterion optimization and multi-criterion decision-making tasks closer together and demonstrated that the proposed iSOM approach can aid in making informed decisions at various stages of the decision-making process by providing DMs a clearer and deeper understanding of the Pareto-optimal solutions.

References

- Branke, J., Corrente, S., Greco, S., Słowiński, R., and Zielniewicz, P. (2016). Using Choquet integral as preference model in interactive evolutionary multiobjective optimization. *European Journal of Operational Research*, 250(3):884–901.
- Branke, J., Greco, S., Słowiński, R., and Zielniewicz, P. (2009). Interactive evolutionary multiobjective optimization using robust ordinal regression. In *International conference on evolutionary multi-criterion optimization*, pages 554–568. Springer.
- Branke, J., Greco, S., Słowiński, R., and Zielniewicz, P. (2015). Learning value functions in interactive evolutionary multiobjective optimization. *IEEE Transactions on Evolutionary Computation*, 19(1):88–102.
- Buchanan, J. T. (1997). A naive approach for solving MCDM problems: The GUESS method. *Journal of the Operational Research Society*, 48(2):202–206.
- Chankong, V. and Haimes, Y. Y. (2008). *Multiobjective decision making: theory and methodology*. Courier Dover Publications.

- Coello, C. A. C., Lamont, G. B., and Van Veldhuizen, D. A. (2007). *Evolutionary algorithms for solving multi-objective problems*, volume 5. Springer.
- Deb, K. (2011). Multi-objective optimisation using evolutionary algorithms: an introduction. In *Multi-objective evolutionary optimisation for product design and manufacturing*, pages 3–34. Springer.
- Deb, K. and Jain, H. (2014). An evolutionary many-objective optimization algorithm using reference-point-based nondominated sorting approach, part I: solving problems with box constraints. *IEEE transactions on evolutionary computation*, 18(4):577–601.
- Deb, K. and Kumar, A. (2007a). Interactive evolutionary multi-objective optimization and decision-making using reference direction method. In *Proceedings of the 9th annual conference on Genetic and evolutionary computation*, pages 781–788.
- Deb, K. and Kumar, A. (2007b). Light beam search based multi-objective optimization using evolutionary algorithms. In *2007 IEEE Congress on Evolutionary Computation*, pages 2125–2132. IEEE.
- Deb, K. and Miettinen, K. (2010). Nadir point estimation using evolutionary approaches: better accuracy and computational speed through focused search. In *Multiple criteria decision making for sustainable energy and transportation systems*, pages 339–354. Springer.
- Deb, K., Pratap, A., Agarwal, S., and Meyarivan, T. (2002). A fast and elitist multiobjective genetic algorithm: NSGA-II. *IEEE transactions on evolutionary computation*, 6(2):182–197.
- Deb, K. and Sundar, J. (2006). Reference point based multi-objective optimization using evolutionary algorithms. In *Proceedings of the 8th annual conference on Genetic and evolutionary computation*, pages 635–642.
- Deb, K. and Talukder, A. K. A. (2021). Visualization-based multi-criterion decision making with NIMBUS method using Palette Viz. In *2021 IEEE Symposium Series on Computational Intelligence (SSCI)*, pages 1–8.
- Gu, F., Liu, H.-L., and Tan, K. C. (2012). A multiobjective evolutionary algorithm using dynamic weight design method. *International Journal of Innovative Computing, Information and Control*, 8(5 (B)):3677–3688.
- Hall, W. A. and Haimes, Y. Y. (1976). The surrogate worth trade-off method with multiple decision-makers. In *Multiple Criteria Decision Making Kyoto 1975*, pages 207–233. Springer.
- Ho, W., Xu, X., and Dey, P. K. (2010). Multi-criteria decision making approaches for supplier evaluation and selection: A literature review. *European Journal of Operational Research*, 202(1):16–24.
- Jaszkiewicz, A. and Słowiński, R. (1999). The ‘Light Beam Search’ approach—an overview of methodology applications. *European Journal of Operational Research*, 113(2):300–314.
- Kadziński, M., Tomczyk, M. K., and Słowiński, R. (2020). Preference-based cone contraction algorithms for interactive evolutionary multiple objective optimization. *Swarm and Evolutionary Computation*, 52:100602.
- Kaliszewski, I., Miroforidis, J., and Podkopaev, D. (2012). Interactive multiple criteria decision making based on preference driven evolutionary multiobjective optimization with controllable accuracy. *European Journal of Operational Research*, 216(1):188–199.
- Karahan, I. and Koksalan, M. (2010). A territory defining multiobjective evolutionary algorithms and preference incorporation. *IEEE Transactions on Evolutionary Computation*, 14(4):636–664.
- Kennedy, M. C., Ford, E. D., Singleton, P., Finney, M., and Agee, J. K. (2008). Informed multi-objective decision-making in environmental management using Pareto optimality. *Journal of Applied Ecology*, 45(1):181–192.
- Kohonen, T. (1997). Exploration of very large databases by self-organizing maps. In *Proceedings of International Conference on Neural Networks (ICNN’97)*, volume 1, pages PL1–PL6. IEEE.
- Köksalan, M. and Karahan, I. (2010). An interactive territory defining evolutionary algorithm: iTDEA. *IEEE Transactions on Evolutionary Computation*, 14(5):702–722.
- Korhonen, P. and Wallenius, J. (1988). A Pareto race. *Naval Research Logistics*, 35(6):615–623.
- Korhonen, P. and Yu, G. Y. (2000). Quadratic Pareto race. In *New Frontiers of Decision Making for the Information Technology Era*, pages 123–142. World Scientific.
- Li, K., Deb, K., Zhang, Q., and Kwong, S. (2014). An evolutionary many-objective optimization algorithm based on dominance and decomposition. *IEEE transactions on evolutionary computation*, 19(5):694–716.
- Li, K., Omidvar, M. N., Deb, K., and Yao, X. (2016). Variable interaction in multi-objective optimization problems. In *International Conference on Parallel Problem Solving from Nature*, pages 399–409. Springer.
- Ma, J., Fan, Z.-P., and Huang, L.-H. (1999). A subjective and objective integrated approach to determine attribute weights. *European Journal of Operational Research*, 112(2):397–404.
- Miettinen, K. (2012). *Nonlinear multiobjective optimization*, volume 12. Springer Science & Business Media.
- Miettinen, K. and Mäkelä, M. (1995). Interactive bundle-based method for nondifferentiable multiobjective optimization: NIMBUS. *Optimization*, 34(3):231–246.
- Miettinen, K. and Mäkelä, M. M. (1996). NIMBUS — Interactive Method for Nondifferentiable Multiobjective Optimization Problems. In *Multi-Objective Programming and Goal Programming*, pages 50–57. Springer Berlin Heidelberg.
- Miettinen, K. and Mäkelä, M. M. (1999). Comparative evaluation of some interactive reference point-based methods for multi-objective optimisation. *Journal of the Operational Research Society*, 50(9):949–959.
- Miettinen, K. and Mäkelä, M. M. (2000). Interactive multiobjective optimization system WWW-NIMBUS on the Internet. *Computers & Operations Research*, 27(7-8):709–723.
- Miettinen, K. and Mäkelä, M. M. (2002). On scalarizing functions in multiobjective optimization. *OR spectrum*, 24(2):193–213.
- Miettinen, K. and Mäkelä, M. M. (2006). Synchronous approach in interactive multiobjective optimization. *European Journal of Operational Research*, 170(3):909–922.
- Miettinen, K., Ruiz, F., and Wierzbicki, A. P. (2008). Introduction to multiobjective optimization: interactive approaches. In *Multiobjective optimization*, pages 27–57. Springer.
- Nagar, D., Ramu, P., and Deb, K. (2021). Interpretable Self-Organizing Maps (iSOM) for Visualization of Pareto Front in Multiple Objective Optimization. In *International Conference on Evolutionary Multi-Criterion Optimization*, pages 645–655. Springer.

- Nakayama, H. and Sawaragi, Y. (1984). Satisficing trade-off method for multiobjective programming. In *Interactive decision analysis*, pages 113–122. Springer.
- Qi, Y., Ma, X., Liu, F., Jiao, L., Sun, J., and Wu, J. (2014). MOEA/D with adaptive weight adjustment. *Evolutionary computation*, 22(2):231–264.
- Simpson, T., Allen, J., Chen, W., and Mistree, F. (1996). Conceptual design of a family of products through the use of the Robust Concept Extrapolation Method. In *6th Symposium on Multidisciplinary Analysis and Optimization*, page 4161.
- Sinha, A., Korhonen, P., Wallenius, J., and Deb, K. (2014). An interactive evolutionary multi-objective optimization algorithm with a limited number of decision maker calls. *European Journal of Operational Research*, 233(3):674–688.
- Siwei, J., Zhihua, C., Jie, Z., and Yew-Soon, O. (2011). Multiobjective optimization by decomposition with Pareto-adaptive weight vectors. In *2011 Seventh international conference on natural computation*, volume 3, pages 1260–1264. IEEE.
- Steuer, R. (1986). *Multiple Criteria Optimization: Theory, Computation, and Application*. Wiley series in probability and mathematical statistics: Applied probability and statistics. Wiley.
- Talukder, A. K. A. and Deb, K. (2020). PaletteViz: A Visualization Method for Functional Understanding of High-Dimensional Pareto-Optimal Data-Sets to Aid Multi-Criteria Decision Making. *IEEE Computational Intelligence Magazine*, 15(2):36–48.
- Thole, S. P. and Ramu, P. (2020). Design space exploration and optimization using self-organizing maps. *Structural and Multidisciplinary Optimization*, 62(3):1071–1088.
- Tomczyk, M. K. and Kadziński, M. (2019). Robust indicator-based algorithm for interactive evolutionary multiple objective optimization. In *Proceedings of the Genetic and Evolutionary Computation Conference*, pages 629–637.
- Vesikar, Y., Deb, K., and Blank, J. (2018). Reference point based NSGA-III for preferred solutions. In *2018 IEEE Symposium Series on Computational Intelligence (SSCI)*, pages 1587–1594.
- Wang, R., Purshouse, R. C., and Fleming, P. J. (2013). Preference-inspired coevolutionary algorithms for many-objective optimization. *IEEE Transactions on Evolutionary Computation*, 17(4):474–494.
- Wang, R., Purshouse, R. C., and Fleming, P. J. (2015a). Preference-inspired co-evolutionary algorithms using weight vectors. *European Journal of Operational Research*, 243(2):423–441.
- Wang, R., Purshouse, R. C., Giagkiozis, I., and Fleming, P. J. (2015b). The iPICEA-g: a new hybrid evolutionary multi-criteria decision making approach using the brushing technique. *European Journal of Operational Research*, 243(2):442–453.
- Wierzbicki, A. P. (1980). The use of reference objectives in multiobjective optimization. In *Multiple criteria decision making theory and application*, pages 468–486. Springer.
- Wierzbicki, A. P. (1999). Reference point approaches. In *Multicriteria decision making*, pages 237–275. Springer.
- Yuan, Y., Xu, H., Wang, B., and Yao, X. (2015). A new dominance relation-based evolutionary algorithm for many-objective optimization. *IEEE Transactions on Evolutionary Computation*, 20(1):16–37.